ABSTRACT

Title of Document: RHENIUM-OSMIUM AGE DETERMINATIONS OF GLACIOGENIC SHALES FROM THE MESOPROTEROZOIC VAZANTE FORMATION, BRAZIL

Nicholas J. Geboy, M.S., 2006

Directed By: Professor Alan Jay Kaufman
Department of Geology

The Vazante Group is a sedimentary package of carbonate interbedded with diamictite and organic-rich shale, potentially representing a Pleistocene-style glacial cycle of Proterozoic age in Brazil. Lacking volcanic ashes, the age of the Vazante strata has eluded researchers. This study applied the Re-Os geochronometer to successive organic-rich horizons, revealing pre- and synglacial ages of *ca.* 1.35 and 1.13 Ga. Time-series stable isotopic studies were conducted throughout the succession to investigate active metabolisms and depositional redox conditions. Given the radiometric constraints, the Vazante Group contains the only recognized glacial deposit of Mesoproterozoic age, but may be similar to Neoproterozoic events. Vazante strata were deposited on a low-latitude passive margin formed during the diachronous break-up of the supercontinent Rodinia, with local ice-sheets potentially developing on uplifted rift margins. A low-latitude Mesoproterozoic glaciation suggests that the "climate paradox" of the Neoproterozoic extends back further than previously believed.

RHENIUM-OSMIUM AGE DETERMINATIONS OF GLACIOGENIC SHALES FROM THE MESOPROTEROZOIC VAZANTE FORMATION, BRAZIL

By

Nicholas J. Geboy

Thesis submitted to the Faculty of the Graduate School of the
University of Maryland, College Park, in partial fulfillment
of the requirements for the degree of
Master of Science
2006

Advisory Committee:
Professor A. Jay Kaufman, Chair
Professor Richard J. Walker
Professor Andrew Campbell

Acknowledgments

I would like to begin by acknowledging the contributions of my family and life-long friends in Wisconsin. Their support and reassurance during my time in Maryland never wavered and helped me get through some of the more difficult moments I have experienced here. My high school geology teacher, Mr. Gerald Gutoski, first introduced me to the science and encouraged me to pursue it in college. With his advisement I was lucky enough to enter into the Geology Department at the University of Wisconsin-Oshkosh, the faculty and staff of which must also be acknowledged. I entered graduate school feeling prepared and this speaks more to their credit than to mine. I would particularly like to thank Dr. Eric Hiatt who provided me with countless research possibilities, career advice, and a friendship that helped keep me centered during my time in Oshkosh. I would like to thank the faculty and staff in the Department of Geology at the University of Maryland, especially Drs. A. Jay Kaufman, Richard Walker, and Andrew Campbell would made this thesis successful and (hopefully) refined. I also thank my fellow graduate students for support, scientific feedback and friendship. Dave Johnston, especially, helped me to transition to Maryland with endless guidance and patience. For this I think him.

This project was funded with NASA Exobiology grant EXB04-0000-0082 and samples were provided by Tolentino Flavio de Oliviera of Companhia Mineira de Metais, Brazil.

Table of Contents

List of Tables

List of Figures

Chapter 1: Introduction

1.1 "Snowball Earth"

During the early Neoproterozoic Era, the São Francisco craton was situated within the supercontinent known as Rodinia, which was long-lived, being in a stable configuration from ~1050 Ma until ~750 Ma (Hoffman, 1999; Eyles and Januszczak, 2004). The exact positioning of the individual continents within Rodinia, however, is debated (see Hoffman, 1999 for review) with some authors even questioning the presence of all cratons within the contiguous landmass (Kroner and Cordani, 2003). There is strong evidence that Rodinia was situated about the equator, with the continents, including the São Francisco craton, within tropical latitudes (Hoffman, 1999) as discussed later. Rodinia's eventual break-up and consequent re-positioning into Gondwana temporally coincides with wide-spread glaciations that ranged from polar to equatorial latitudes (Evans, 2000).

1.1.1 Low-Latitude Glacial Events

At either end of the Proterozoic Eon, a series of potentially global low-latitude glaciations occurred, which left behind deposits of glacial diamictite as well as texturally and isotopically unique cap carbonate (Harland and Bidgood, 1959; Kaufman *et al.*, 1991; Kirschvink, 1992; Kennedy, 1996; Hoffman *et al*., 1998; Schrag *et al*, 2002; Bekker *et al*., 2005). In some models these widespread ice ages are believed to have resulted in completely frozen equatorial oceans (Kirschvink, 1992; Hoffman *et al*., 1998;

Hoffman and Schrag, 2002), which would have had dramatic effects on the atmosphere, hydrosphere, and biosphere. Specifically, the Neoproterozoic (1000-543 Ma; Plumb, 1991; Bowring *et al.*, 1993) had multiple low-latitude glacial events, with the literature citing two to four or more discrete episodes (*cf.* Kaufman *et al.*, 1997; Kennedy *et al.*, 1998; Walter *et al.*, 2000). Assuming these glacial episodes are global in scope, Schrag and others (2002) suggest it is only important that the community agrees that there were multiple events (regardless of how many) because this indicates that the conditions needed to initiate the glaciations had to have persisted across most of the Neoproterozoic Era. Knoll *et al.* (1986) first suggested the break up of Rodinia as a possible trigger for the ice ages. These authors hypothesized that supercontinent fragmentation would increase sedimentation rates and burial of organic matter, thereby creating a carbon sink. Productivity blooms prior to the ice ages would provide a direct pump of atmospheric CO_2 out of the system (Kaufman *et al*., 1997). With increased burial effectively removing carbon from the system, less would be available to be reoxidized to atmospheric CO_2, thereby cooling the globe. Carbon isotopes support this hypothesis in that carbonates deposited prior to ice ages are strongly enriched in ^{13}C, suggesting higher proportional organic carbon production and burial removing ^{12}C from the system (Kaufman *et al.*, 1997). Following the ice ages, carbonates are depleted in ^{13}C, possibly caused by upwelling of waters where the buried organic matter had been remineralized (Kaufman *et al*., 1997). Schrag *et al.* (2002) alternatively proposed that the location of the continents on the equator (a condition that existed throughout most of the era) caused the glaciations. The theory stated that once ice extends past a critical latitude (40-30°), the rate of increase of planetary albedo would cause a runaway ice house and extension

of the ice line to the equator. Figure 1 (after Schrag *et al.*, 2002) illustrates the affect of having all the continents at low latitudes. Weathering of continental silicate material is a sink for atmospheric CO_2. Therefore, when continents are covered with glaciers they are unable to act as this sink and atmospheric CO_2 builds up, warming the globe and causing glacial retreat. If all continental silicate material is situated on or near the equator, polar glaciers can advance without removing this CO_2 sink. Eventually the glaciers would advance past a critical latitiude, plunging the earth into icehouse period (Schrag *et al.*, 2002).

Atmospheric CO_2 would need to reach a critical concentration of ~120,000 ppm to escape from snowball Earth conditions (Caldeira and Kasting, 1992). Hoffman and others (1998b) argue that with silicate weathering, ocean-atmosphere exchange, and primary productivity all effectively diminished, there would be no carbon sinks from the atmosphere and continued pumping of volcanogenic CO_2 would build up during the glaciation until it breeched the ~120,000 ppm threshold. The Earth would warm rapidly due to the non-linear relationship between CO_2 and greenhouse forcing, and from dramatically increased rates of evaporation bringing much more water vapor into the atmosphere (Caldiera and Kasting, 1992).

1.1.2 Duration of Low-Latitude Glacial Events

Previous studies have attempted to determine the duration of these ice age events by a variety of sedimentalogical and geochemical models. For example, on some continents Neoproterozoic glacial diamictites are sandwiched between thick shallow marine carbonates, which record strong positive-to-negative trends in carbon isotopic

composition (Kaufman and Knoll, 1995; Kaufman *et al*., 1997; Hoffman *et al*., 1998a). In the Otavi Group of Namibia, the cap-carbonate of the Maieberg Formation (overlying the Ghaub Formation diamictite), contains negative $\delta^{13}C$ values throughout and shows no evidence of subareal exposure for over 400 meters. This negative carbon isotope anomaly may be interpreted to reflect severely limited marine photosynthesis (Hoffman *et al*., 1998b), the release of methane from the seafloor (Kennedy *et al*., 2001), or extreme rates of carbonate deposition (Kaufman *et al*., in preparation). Hoffman *et al*. (1998a) used the stratigraphic extent of this excursion and a thermal subsidence model to estimate that the Ghaub glaciation may have lasted ~9 Ma.

Accepting this constraint on the duration of the ice age and the biogeochemical anomaly, Hoffman *et al*. (1998a) then considered the timing of long term buildup of atmospheric CO_2 needed to ultimately escape such an extreme icehouse state. Assuming little to no ocean-atmosphere exchange, it would take at least four million years to build up to 120,000 ppm level of CO_2, with 30 Ma as an upper estimate (Hoffman *et al*, 1998b).

Recently, iridium (Ir) anomalies in post-glacial cap carbonates in central Africa have been used to determine the duration of a Neoproterozoic glacial event. In this case, if there were frozen tropical oceans, interplanetary dust particles (IDP's) would have accumulated on the ice, rather than entering the marine system. During the subsequent warming, the glaciers would retreat and the IDP's would rain to the ocean floor and accumulate rapidly in the first sediments deposited after the glaciers receded. Bodiselitsch and others (2005) measured an Ir anomaly (almost 2 ppb against a background of <0.5 ppb) at the base of cap carbonate and modeled that three million, and

more likely 12 million, years would be necessary to concentrate the Ir measured in the excursion. Constraints on this result may come from the measurement of a stratigraphic suite of PGE elements in diamictite and cap carbonate lithofacies; such tests may not be conclusive, however, as estimates of sedimentation rate must be determined to guide sampling of appropriate volumes of rock for such analysis.

Direct U-Pb radiometric constraints on zircons in volcanic ash levels beneath, within, and above a terminal Neoproterozoic ice age preserved in Newfoundland indicate that all three occurred within the 1 Ma uncertainty on analyses of deposits *ca*. 585 million years old (Bowring *et al*., 2003). Advocates of the Snowball Earth suggest that while this terminal Neoproterozoic glacial event may not have been global, earlier Marinoan and Sturtian events (*ca*. 635 and 712 Ma, respectively) were. Direct radiometric age dates provide the most valuable temporal constraints on events in Earth history, but volcanic ash layers are relatively rare in the sedimentary record. Black shales, however, are not as uncommon. Black shales have been found in association with Proterozoic glacial deposits in Australia (Schaefer and Burgess, 2003; Kendall *et al*., 2006), Canada (Kendall *et al.*, 2004) and Brazil (this study). The application of rhenium-osmium geochronometry to glaciogenic black shales offers an opportunity to sufficiently precisely determine depositional ages, thereby allowing for more precise timing of low-latitude ice age events. In addition, it allows for dating geologic units at a finer scale allowing time series stable isotope trends to be placed into context. For this tool to be applicable, however, excellent precision and closely spaced dates must be obtained, as interpreting trends spaced millions of years apart is unrealistic.

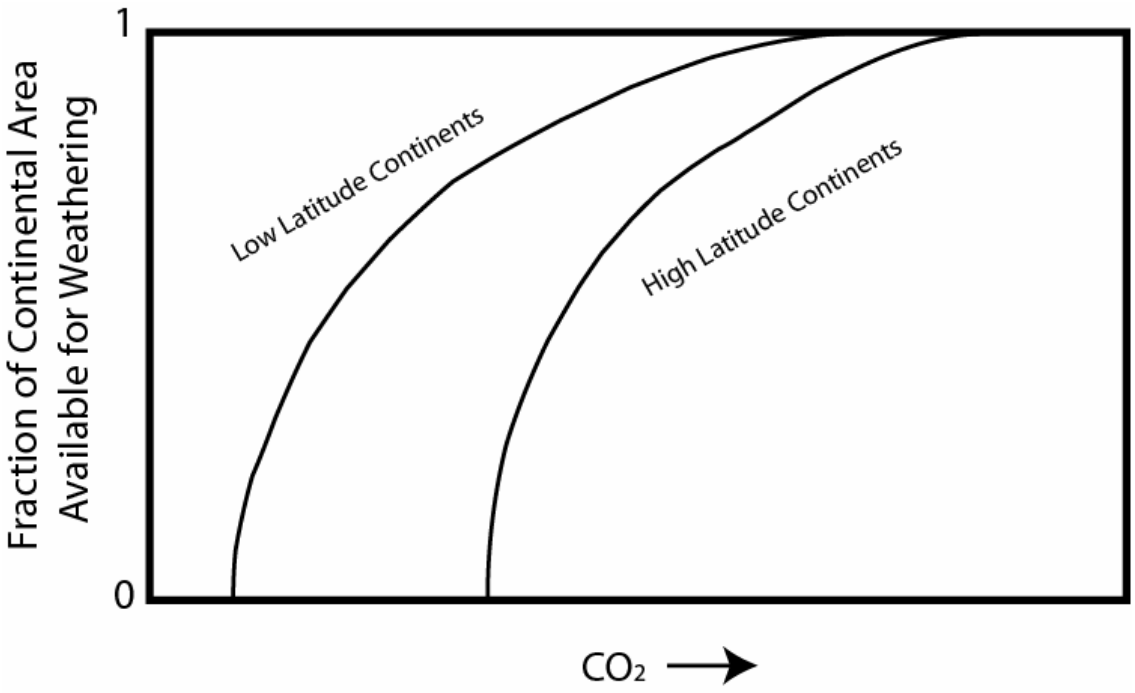

Figure 1. Atmospheric carbon dioxide concentrations drop as continents weather. This cools the globe creating ice sheets which limit the amount of continental area available to be weathered. Positioning the continents on the equator disrupts this stabilizing effect and can plunge the Earth into a global glaciation (Modified from Schrag et al., 2002).

1.2 Re-Os Systematics

1.2.1 Characteristics and Terminology

The rhenium-osmium system is characterized by long-lived ($t_{1/2}$ of 41.6 Ga) negatron decay of ^{187}Re to ^{187}Os (Shirey and Walker, 1998). Rhenium is a refractory metal with two isotopes, ^{185}Re and ^{187}Re (Dickin, 1995). The heavier radioactive isotope accounts for 62.6% of total rhenium. Osmium is a platinum group element (PGE) with seven isotopes: ^{184}Os, ^{185}Os, ^{186}Os, ^{187}Os, ^{188}Os, ^{190}Os, and ^{192}Os. Osmium has no fixed atomic mass or absolute abundance of its isotopes because two of them are radiogenic (Shirey and Walker, 1998). Osmium-187 is the radiogenic daughter of ^{187}Re and ^{186}Os is the daughter isotope from alpha decay of ^{190}Pt (Dickin, 1995).

Rhenium is a moderately incompatible element, geochemically most similar to molybdenum. It therefore readily partitions into the melt phase during crust formation. This behavior leads to high concentrations of rhenium in mid-ocean ridge basalts (MORB; 0.5-2 ppb) relative to lesser mantle concentrations (0.051-0.30 ppb; Shirey and Walker, 1998). On the other hand, osmium is highly compatible (Dickin, 1995). It is therefore concentrated in the mantle (0.8-9 ppb) relative to MORB (0.001-0.05 ppb; Table 1; Shirey and Walker, 1998). This fractionation of rhenium from osmium during crust formation causes crustal sources of osmium to be much more radiogenic (enriched in ^{187}Os) than mantle sources. Both of these elements, however, are considered highly siderophile (iron-loving) and chalcophile (sulfur-loving), leading towards nearly quantitative extraction into the core (Shirey and Walker, 1998). This behavior also

allows for higher concentrations of both rhenium and osmium in sulfide minerals (Shirey and Walker, 1998).

Os isotopic compositions are often expressed in gamma-notation where:

$$\gamma_{Os(t)} = \{[(^{187}Os/^{188}Os_{sample(t)})/(^{187}Os/^{188}Os_{chondrite(t)})]-1\} \times 100$$

This notation signifies the percent deviation of a sample from chondrite at a specific time (Shirey and Walker, 1998). Samples with positive γ_{Os} are radiogenic (or enriched) in that they have evolved towards a higher $^{187}Os/^{188}Os$ ratio than the chondritic average over time. Conversely, samples with negative γ_{Os} are non-radiogenic (or depleted).

Another term used with respect to the Re-Os system is a model age, or T_{DM}. This is the time since the sample departed from the depleted mantle. That is, assuming the sample had an initial mantle value prior to becoming part of the crust, T_{DM} is how long must take for the sample to evolve to its current isotopic composition.

1.2.2 Applications of Re-Os

The Re-Os isotope system offers unique applications in high-temperature geochemistry and cosmoschemistry. Many of the common isotope systems (i.e. Rb-Sr, Sm-Nd, U-Pb, etc.) are lithophile elements, leading to extremely low concentrations in metals in general, and specifically in meteorites (Shirey and Walker, 1998). On the other hand, both rhenium and osmium have an affinity for metals and sulfides, so this system can be applied to evolution of the mantle, the origin of PGE-bearing ore deposits and early solar system events (Shirey and Walker, 1998). Since the decay constant of ^{187}Re

to ^{187}Os is relatively well-constrained, the system can also be used to date these metal-bearing systems.

The Re-Os geochronometer has also been successfully used to date shales that contain from <1 to >10% organic carbon (Ravizza and Turekian, 1989; Cohen *et al.*, 1999; Creaser *et al*., 2002; Kendall *et al.*, 2004; Selby and Creaser, 2005; Kendall *et al.*, 2006). Organic rich shales are generally thought to be deposited in anoxic environments, and this anoxia also leads to sequestration of rhenium and osmium from seawater, insofar that these elements are relatively immobile in their reduced states (Cohen *et al.*, 1999). Redox reactions located at or below the sediment-water interface concentrate hydrogenous rhenium and osmium (Kendall *et al*., 2004), which are then sequestered from seawater and syndepositionally incorporated into the mudrock, often associated with organic material (Selby and Creaser, 2003). Following incorporation, ^{187}Re decays to ^{187}Os with a half life of ~42 Ga; this geochronometer has been successfully used to determine depositional ages of Paleoproterozoic syndepositional pyrites (Hannah *et al.*, 2004) to Jurassic mudstones (Cohen *et al.*, 1999). It is normally assumed that shale remains closed due to its general impermeability. If the non-hydrogenous component is negligible, the Re-Os system can be applied to any mudrock with significant organic matter. Determination of total organic carbon abundances is therefore necessary in the evaluation of a potential sample sets. Samples with more preserved organic carbon are more likely to host other reduced species, i.e., rhenium and osmium. If the non-hydrogenous component is significant, an alternate digestion medium may be applied during sample processing (see Methods).

1.2.3 Isochron Generation

A precise isochron requires that all samples have the same initial osmium isotopic ratio, and a large spread in parent:daughter ratios. An isochron is a plot of $^{187}Re/^{188}Os$ on the x-axis versus $^{187}Os/^{188}Os$ on the y-axis. If all samples have the same initial $^{187}Os/^{188}Os$ and varying amounts of parent to daughter, they will form a horizontal line at the time of deposition and evolve upward on the plot at different rates. The slope of this line will reveal the age of the suite, and the y-intercept will reveal the initial $^{187}Os/^{188}Os$ of the system (Fig 2). Osmium isotopes are normally measured relative to ^{188}Os. Rhenium is measured for both of its isotopes at masses 185 and 187. This technique has previously been applied to post-glacial Neoproterozoic shales. Schaefer and Burgess (2003) determined the age of some rocks of the Aralka Formation of central Australia to be 592±14 Ma. This age was generated using an inverse aqua-regia digestion and included only three data points. Kendall (2006) used a more selective chromic oxide-sulfuric acid digestion medium (targeting only hydrogenous components) on Schaefer and Burgess' sample suite and derived an age of 657.2 ± 5.4 Ma with a five point isochron. This discrepancy suggests the terrigenous component is not always negligible and precaution must be taken. Kendall and others previously dated another Proterozoic post-glacial deposit using the Re-Os geochronometer. In their 2004 study, the authors placed an age of 607.8±4.7 Ma on the Old Fort Point Formation of Western Canada. The authors digested their samples using both mediums. While the resulting ages are statistically identical, one can see the better precision obtained using the chromic oxide-sulfuric acid technique as the MSWD of the regression falls from 65 to 1.2 (Figure 3). The difference between digestion mediums are outlined in the Methods section.

As mentioned above, the y-intercept of an isochron is the initial osmium isotopic composition of the samples. In the case of organic-rich sediments, this value is interpreted as the osmium isotopic composition of seawater (Ravizza and Turekian, 1989). Osmium exists at very low concentrations (pg/kg) in the oceans (Levasseur *et al*., 1998), but has limited sinks. The only known sink for osmium from the global oceans is marine sedimentation (Oxburgh, 2001). Ravizza and Esser (1993) estimate a global osmium flux of ~90 kg/yr for anoxic basins, metalliferous sediments and pelagic sediments. Oxburgh (2001) estimates an additional 40-60kg/yr of osmium are buried within marine carbonates. A more significant (but less constrained) sink for marine osmium is organic-rich sediment that is not anoxic. Oxburgh (2001) estimates this process removes 130-1100kg/yr of osmium from the oceans. This flux is difficult to constrain because the mechanism by which osmium is incorporated into organic-rich sediments is not well understood. While the residence time of osmium in the oceans is debated (different values are presented in a summary by Peucker-Ehrenbrink and Ravizza, 2000), it is agreed that it is longer than the mixing time of the oceans (~40 ka residence time vs. 2-3 ka oceanic mixing time; Cohen, 2004). Therefore osmium is isotopically uniform in the oceans at any given instant. It does, however, vary greatly with time. Figure 4 shows the osmium seawater curve for the Cenozoic to illustrate this point. Hannah and others (2004) dated syndepositional pyrites at *ca.* 2316 Ma with an initial Os value of 0.1121±0.0012. The authors interpret this chondritic value to reflect the atmosphere's inability to oxidize (i.e. mobilize) crustal osmium sources, thus, mantle sources dominate the signature. Currently, the osmium isotopic composition of seawater is the highest it has ever been with a value of 1.06 (Levasseur *et al.*, 1998; Burton *et al.*,

1999; Woodhouse *et al.*, 1999). It is then expected that initial osmium isotopic values for Proterozoic samples should likely fall somewhere between the Paleoproterozoic, non-radiogenic 0.112 and modern 1.06 values. It is difficult to be more precise in expected initial osmium values as the Proterozoic curve is extremely poorly defined with only one datum for the Paleoprotozoic (Hannah *et al.*, 2004), two in the Mesoproterozoic (from this study) and three from the Neoproterozoic (Kendall *et al.*, 2004; 2006).

Table 1. Concentration of rhenium and osmium in various lithospheric reservoirs. Note the abundance of both Re and Os in black shales relative to other crustal sources (values from Shirey and Walker, 1998).

	Re (ppb)	Os (ppb)	$^{187}Re/^{187}Os$
Fertile Mantle	0.25-0.30	2.8-3.4	0.401
Depleted Mantle	0.051-0.135	0.8-9	0.06-1
MORB	0.5-2	0.001-0.05	100-5000
OIB	0.1-1	0.01-0.5	20-3000
Average Continental Crust	<1	<0.05	~50
Black Shales	517	2.46	18780

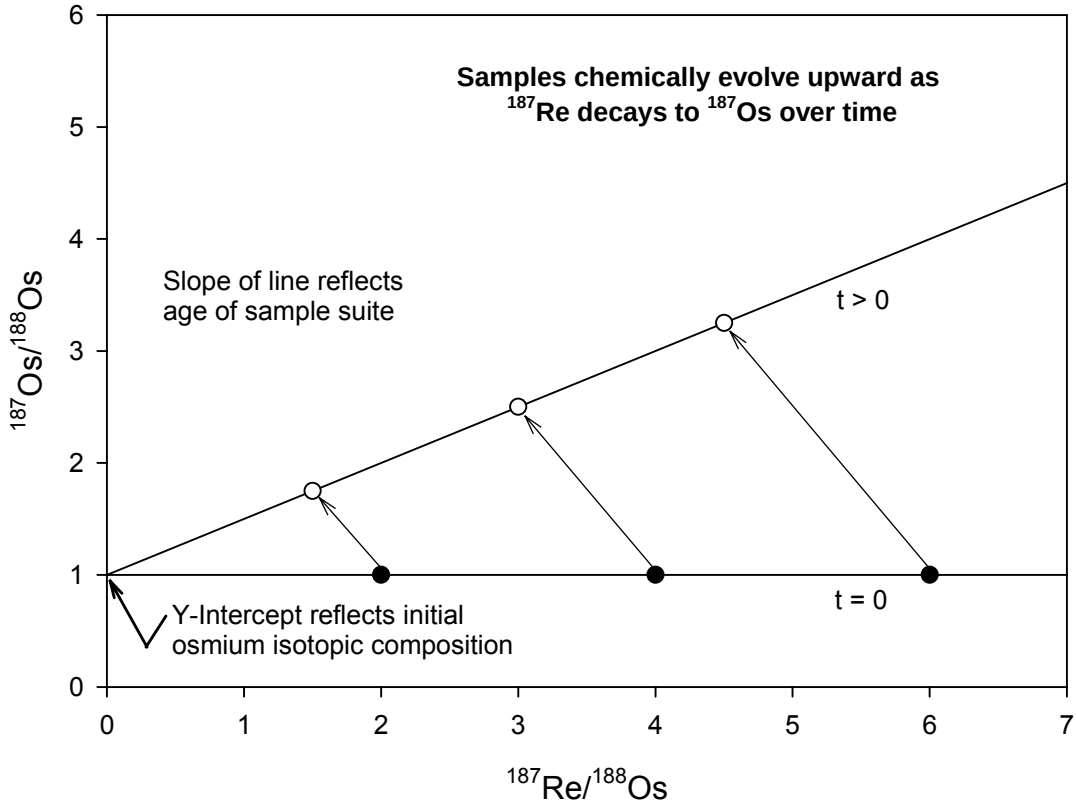

Figure 2. Initally, all samples plot on this graph as a horizontal line. With time (as rhenium-187 decays to osmium-187) the points evolve upward and to the left. The slope of the line at any point reveals the age of the sample set. Note the y-intercept value does not change with time.

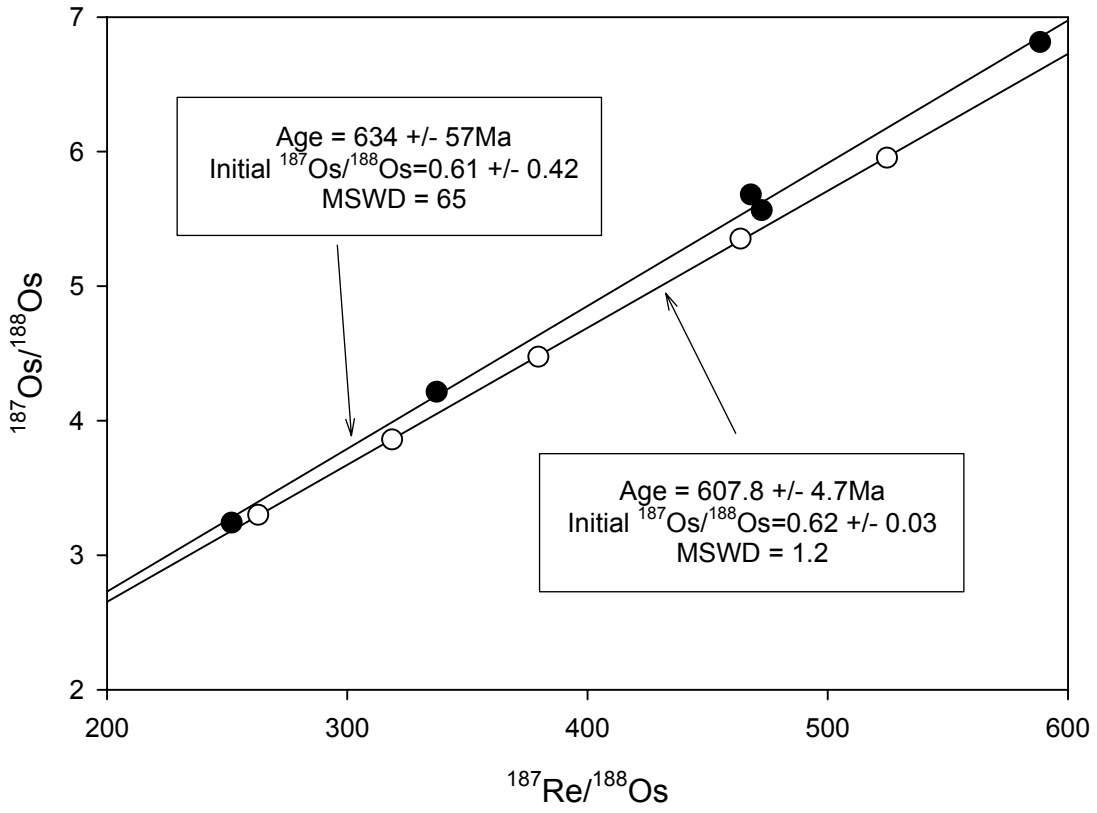

Figure 3. Two isochrons made from the sample set. The closed symbols represent those samples digested using inverse aqua regia. Open symbols are those digested using chromic oxide-sulfuric acid. While the ages are statistically identical, the precision is much better using the chromic oxide solution (data from Kendall *et al.*, 2004).

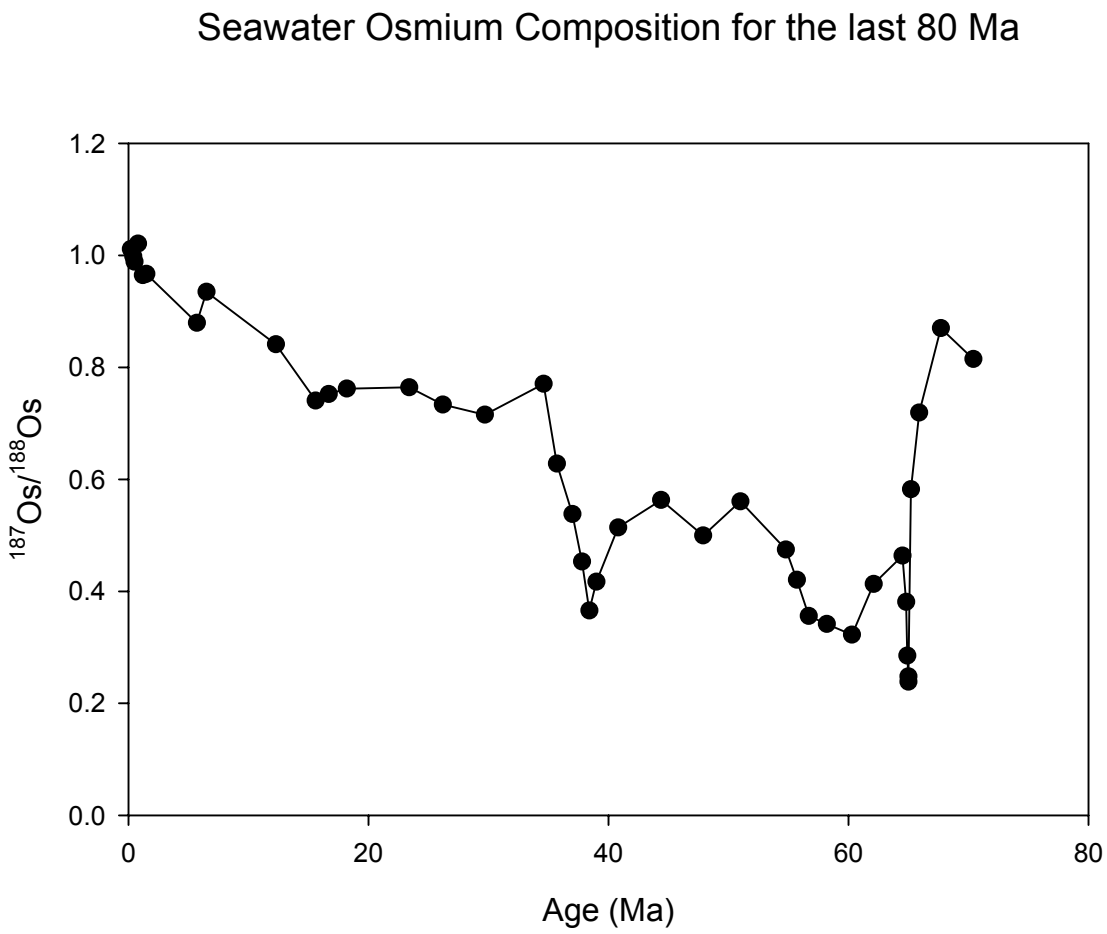

Figure 4. Osmium isotopic composition of the oceans over the past 75 Ma (data from Peucker-Ehrenbrink *et al.*, 1995).

1.3 Geologic Background

1.3.1 The Vazante Group

The Vazante Group is a carbonate and black shale-rich sedimentary package interpreted to have been deposited before, during and following the Sturtian glacial event (Azmy *et al.*, 2001; 2006; Olcott *et al.*, 2005). It is situated in Minas Gerias, Brazil along the eastern part of the Brasília fold belt on the western margin of the São Francisco Craton (Fig. 5). The sedimentary succession includes, from the base, the Serra do Garrote Formation, the Serra do Poço Verde Formation, and the Lapa Formation (Fig. 6). It is important to note that the Vazante Group displays up to seven identified formations in some localities, but only the three afore-mentioned are of relevance to this thesis (Fig. 7; see Babinski *et al*., 2005 for a more comprehensive discussion).

The pre-glacial Serra do Garrote Formation overlies the São Francisco Craton in east-central Brazil and consists of organic-rich shale and lithic wacke that have been metamorphosed to slate in some regions (Azmy *et al*., 2001). Overlying the Serra do Garrote is the Serra do Poço Verde Formation. This formation is mostly microbial dolomudstone, interpreted to have been deposited in inter- to supratidal environments; the carbonates have been completely dolomitized, yet carbon isotopes are believed to retain their original signature (Azmy *et al*., 2001). Within the shales are discrete layers of diamictites that contain dropstones (Fig. 8; Olcott *et al.*, 2005). These larger clasts truncate the laminations within the organic-rich mudstone matrix, supporting the view that these deposits are ice-rafted debris. The organic-rich mudstones have been interpreted to be deposited on the continental shelf during one of the Neoproterozoic

glacial events, while glacial debris rained down. Further evidence for synglacial deposition is the appearance of glendonite within the mudstones (Fig. 9; Olcott *et al*., 2005). Glendonite is a pseudomorph after ikaite, a cold water carbonate mineral that precipitates in organic-rich sediments at a temperature range of -1.9° to 7°C (James *et al*., 2005). There is variable expression of the shaley units interbedded within the dimaictites between the three drillcores used in this study, possibly suggesting waxing and waning of ice sheets (Fig. 6) in a Pleistocene style of climate change.

The Lapa Formation unconformably overlies the Serra do Poço Verde Formation. The Lapa consists of dolomites with organic-rich mudstone lenses, and is interpreted to be deposited during post-glacial transgression. There are no good constraints on the temporal duration of the unconformity, but the lithologic transition above dropstone-laden diamictite, coupled with a characteristic negative carbon isotopic signature, suggest that the Lapa Formation is a cap carbonate lithofacies (Brody *et al*., 2004; Azmy *et al*., 2006).

There are many controversies regarding the regional and temporal context of the Vazante Group. Dardenne (2000) suggests the Vazante strata represent deposition into a rapidly subsiding basin in the Brasília fold belt's initial thrust fronts *ca.* 790 Ma. In contrast, Pimentel and others (2001) interpret the Vazante Group to be the upper sequence of a continental passive margin deposited following the first stage of diachronous rifting of Rodinia at *ca.* 900 Ma. The appearance of *Conophyton metula Kirichenko* constrains the age from 1350 to 950 Ma (Cloud and Dardenne, 1973). Whole rock Rb-Sr ages for Vazante shales yield an isochron age of ~600 Ma, but this may represent a closing time for the Brasiliano metamorphic event (Amaral and Kawashita,

1967). More recently, Azmy *et al.* (2001) suggest the strontium, carbon and sulfur isotopes are consistent with Sturtian signatures, but this is speculative insofar as the baseline for Precambrian chemostratigraphy is poorly known (*cf*. Babinski *et al.*, 2005) and the Sr isotope constraint come from one single analysis of a dolomitic carbonate in the Lapa Formation. Measuring rhenium and osmium in the underlying organic horizons of the Vazante Group may allow direct radiometric ages to more precisely determine periods of deposition and provide insight into possible regional settings.

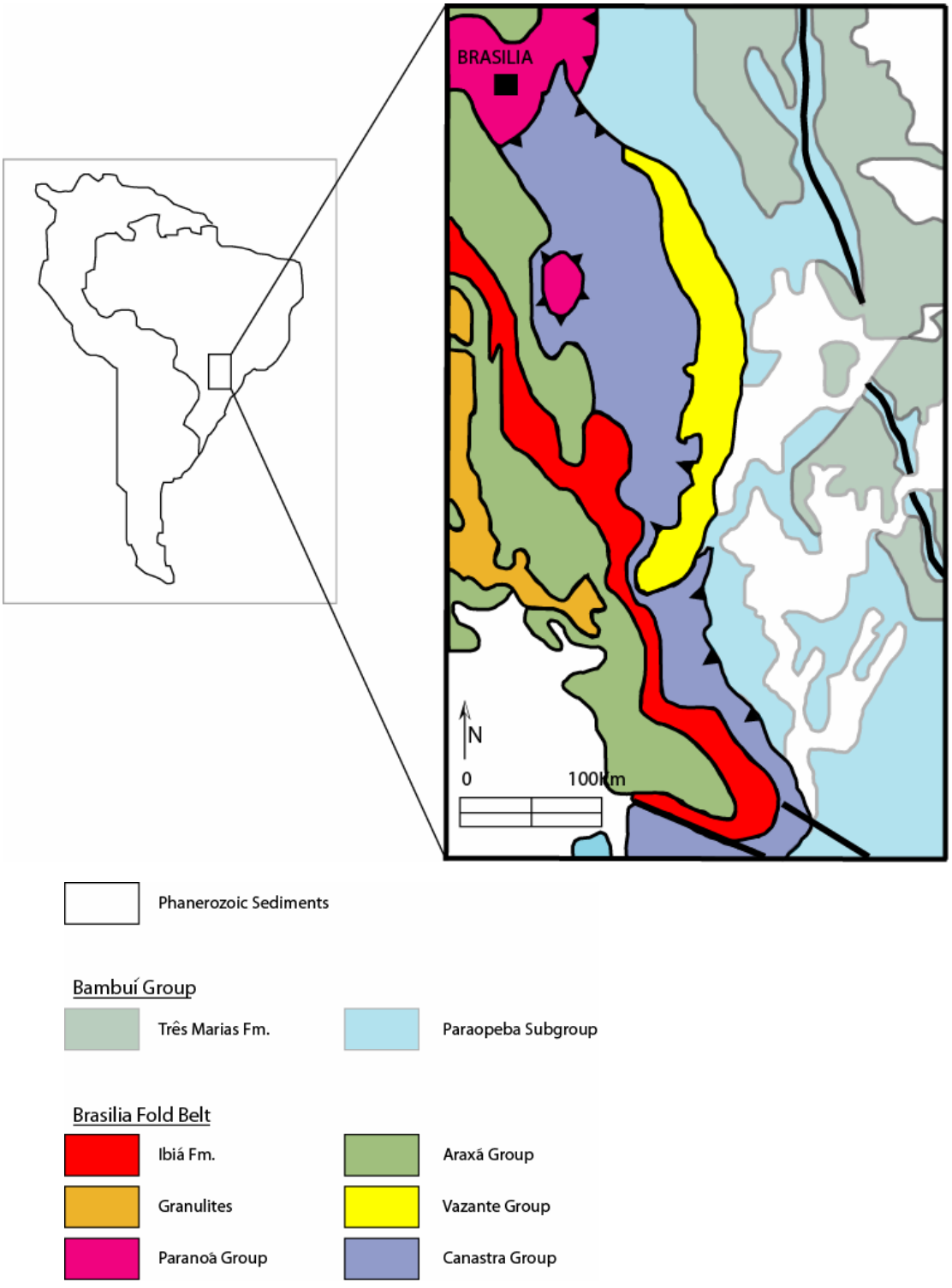

Figure 5. Geologic map of Brasilia Fold Belt. Vazante Group is shown in black (Modified from Babinski *et al.*, 2005).

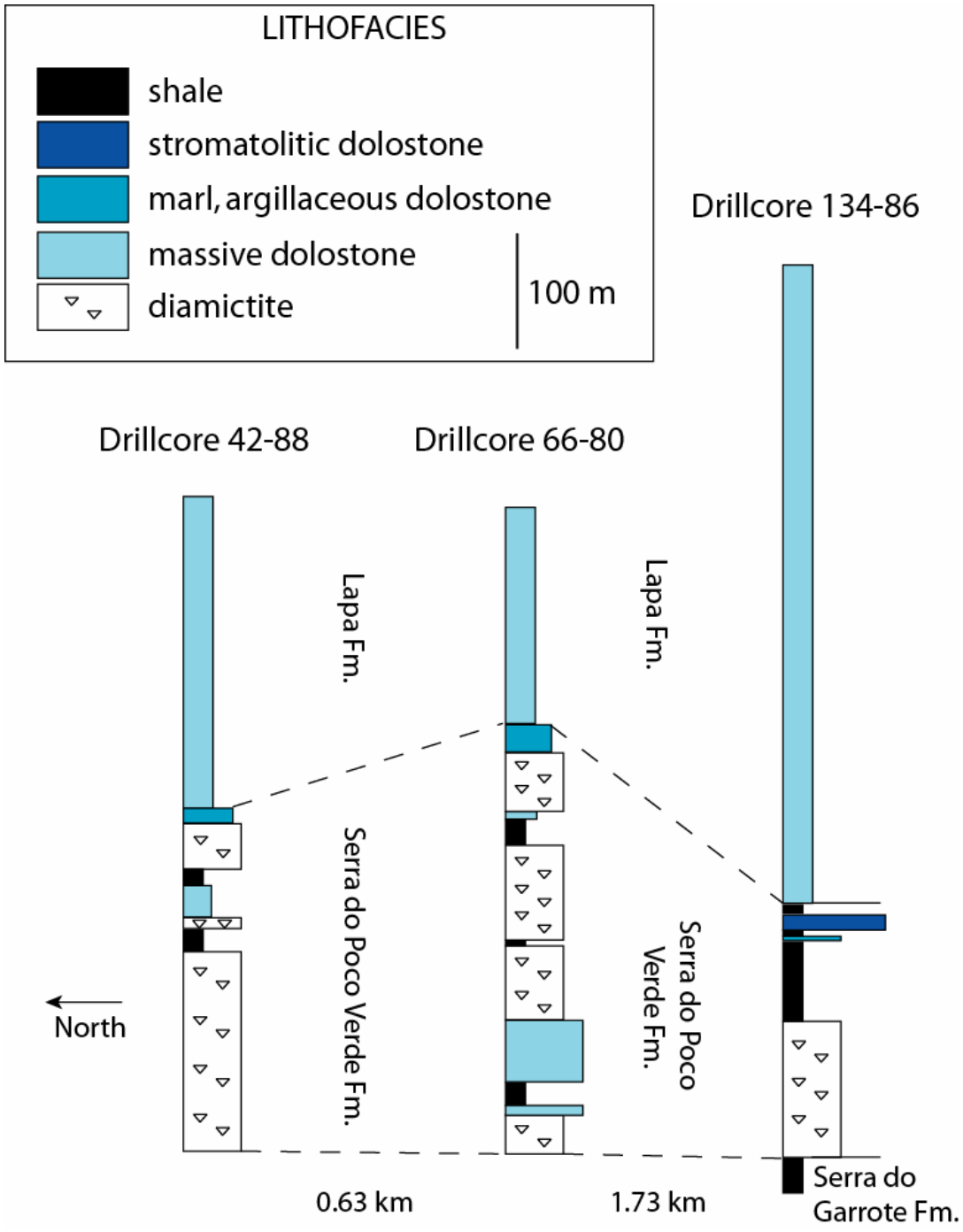

Figure 6. Generalized stratigraphic columns of drill cores sampled.

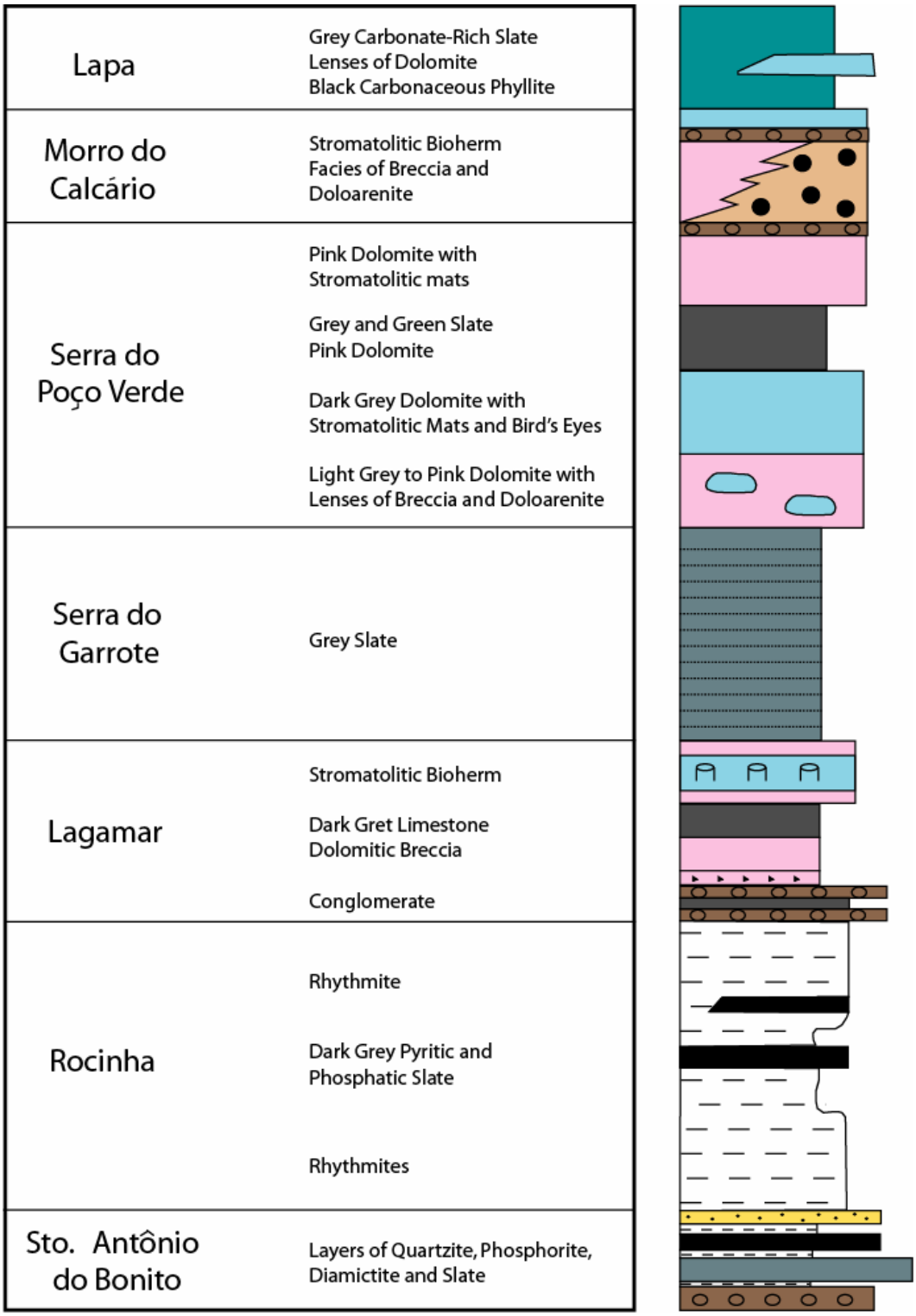

Figure 7. Complete stratigraphic representation of the Vazante Group. Only the Serra do Garrote, Serra do Poço Verde and Lapa Formations are of relevance to this study (modified from Babinski et al., 2005 after Dardenne, 2000).

Figure 8. A carbonate dropstone in an organic-rich mudstone matrix.

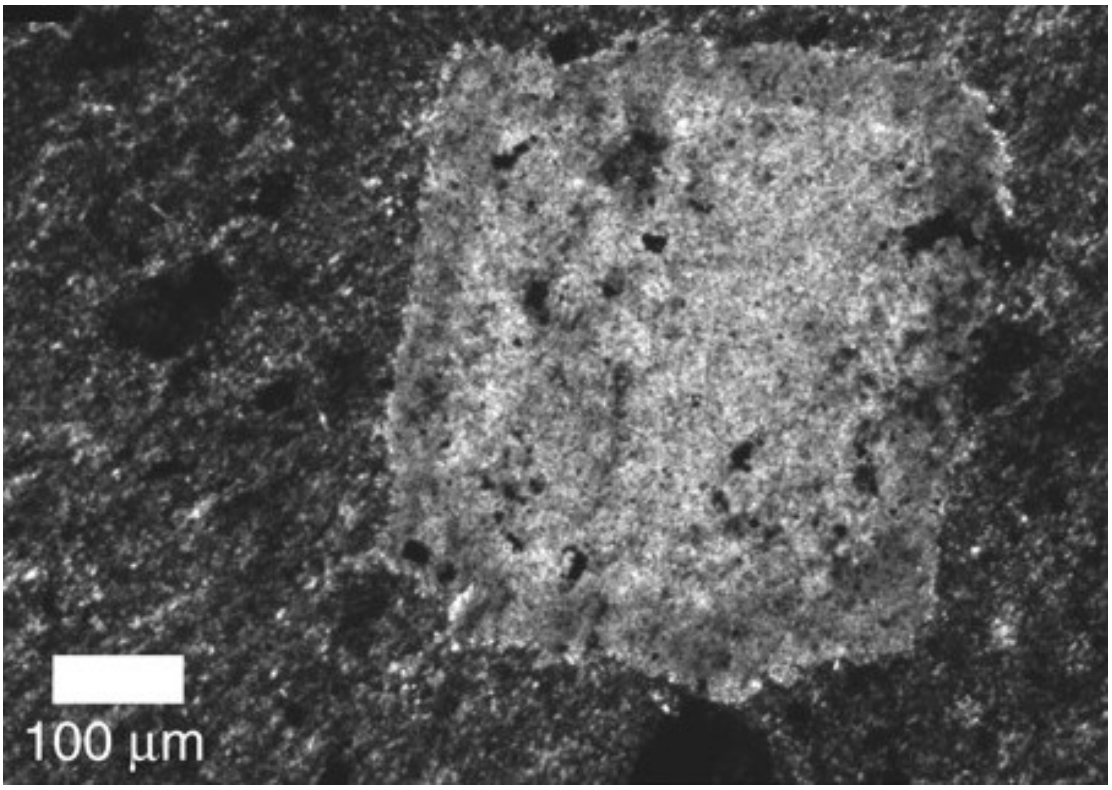

Figure 9. Glendonite, a pseudomorph of ikaite (a cool water carbonate) within the mudstones of the Serra do Poço Verde Fm. (from Olcott *et al*., 2005).

1.4 Carbon and Sulfur

Time series of carbon and sulfur abundances and isotopic compositions can provide context of environmental change across the Serra do Poço Verde. For example, carbon and sulfur stable isotopes offer insight into the degree of bacterial activity in ancient systems. During photosynthesis, cyanobacteria selectively fix the lighter carbon isotope, ^{12}C (Faure, 1991). If the system is carbon-limited (i.e. during rapid growth or low ambient pCO_2) bacteria are forced to incorporate all available carbon, including ^{13}C (Fenchel *et al*., 1998). Carbon isotope compositions are expressed in delta-notation where:

$$\delta^{13}C = 1000*[((^{13}C/^{12}C_{sample})/(^{13}C/^{12}C_{VPDB}))-1]$$

with VPDB being a recognized international standard of Vienna PeeDee belemnite. Measuring isotopically heavy carbon signatures (i.e., more positive than expected $\delta^{13}C$ values) in organic matter may indicate high rates of primary productivity and associated release of O_2, as well as efficient burial of that organic matter.

Likewise, some bacteria reduce sulfate to sulfide, preferentially incorporating the lighter isotopic species, $^{32}SO_4^{2-}$(Faure, 1991). Similar to the carbon system, during periods of rapid sulfate reduction or low sulfate availability, the heavier isotope, $^{34}SO_4^{2-}$, is also reduced (Fenchel *et al*., 1998; Habicht and Canfield, 2001). Sulfur is also denoted using delta notation where:

$$\delta^{34}S = 1000*[((^{34}S/^{32}S_{sample})/(^{34}S/^{32}S_{VCDT}))-1]$$

with VCDT being a recognized international standard of Vienna Canyon Diablo Troilite. Sulfur-34 enriched pyrite may reflect a system in which sulfate reducing bacteria thrived and ^{32}S enriched sulfide was sequestered in sediments. Since carbon-fixing autotrophic organisms create oxidizing environments, and sulfur reducing bacteria are obligate anaerobes requiring anoxic environments, comparing carbon and sulfur data can also offer potential interpretations of the oxidation state of the water column, as well as the boundary conditions of the system.

Chapter 2: Methods

2.1 Sampling

Samples were collected on site in Minas Gerais, Brazil. Organic-rich shales were taken from three individual cores which intersected the same lithologies over several square kilometers (Figs. 6 and 10). Samples from sub-surface drillcores are preferred over outcrops that are exposed at the surface and highly weathered. Mudstone outcrop samples are easily eroded and oxidized, with great loss of initial organic carbon (within which Os and Re are complexed). Weathered shales are shown to exhibit up to ~77% less organic carbon relative to unweathered portions of the same outcrop (Jaffe *et al.*, 2002). The same study found that rhenium and osmium mobility cause weathered samples to have different isotopic signatures relative to unweathered examples. Weathering is a major factor in desert areas like Namibia and South Australia where evidence for low-latitude Neoproterozoic glacial deposits have been discovered.

On the other hand, while weathering alters Re-Os isotope systematics, low levels of thermal maturation apparently do not. Creaser *et al*. (2002) found temperatures up to ~150°C had no effect on rhenium and osmium isotope compositions. Similarly, Kendall *et al*. (2004) found no apparent effect on the Re-Os isotope systematics of shales that were exposed to chlorite-grade metamorphic conditions. Drillcore samples are therefore preferable to measure accurate and precise isotopic compositions.

While there is evidence the Vazante shales have been thermally matured, there is no indication they have seen temperatures higher than chlorite-grade metamorphism; chlorite within the black shales sampled are restricted to fractures and most likely a result

of fluid movement restricted to those pathways. Sample sets were identified within the cores by darkness (to ensure organic-richness) and vertical proximity (to ensure similar initial osmium isotopic composition).

2.2 Total Organic Carbon (TOC)

TOC is measured by Dumas combustion techniques and quantified on a vacuum distillation line. Powdered samples are accurately weighed (between 30 and 130 mg depending on the "darkness" of the powder) and loaded into annealed Vycor tubing. The samples are then acidified with 12N HCl and then centrifuged and decanted (2x) to remove all carbonate carbon. Following acidification the samples are rinsed with Milli-Q water, centrifuged, decanted and dried. Once dry, approximately 1g of cupric oxide is added and the tubes are sealed under vacuum. The samples are combusted at 850°C for two hours. The cupric oxide in the sealed tube is reduced while the organic carbon is oxidized into CO_2 gas. After cooling, the samples are attached to the distillation line. Once cracked, the gaseous contents pass through a water trap of ethanol/dry ice slurry and a CO_2 trap of liquid nitrogen. The CO_2 trap is then isolated and warmed. The internal pressure is displayed on a Baratron readout and converted to μmols using a calibration curve. TOC is determined as a weight percent using the μmols CO_2 and initial mass of bulk sample.

2.3 Re-Os Analysis

Re and Os are oxidized using carius tube digestion as outlined in Shirey and Walker (1995). Two digestion mediums are used. Inverse aqua regia (2:1 concentrated

nitric acid to concentrated hydrochloric acid) has traditionally been used to digest matrices and oxidize both rhenium and osmium to their highest valence states (+7 and +8, respectively). Aqua regia is a strong digestion medium that dissolves the entire sample with the possible exception of quartz (Selby and Creaser, 2003). Precise measurements of black shale require a slightly less aggressive digestion medium; this is because black shales have a hydrogenous component (sequestered from seawater) and a terrigenous component (detrital input). The detrital input can have vastly different signatures from the seawater input, thus skewing measured results. Using CrO_3-H_2SO_4 solution, both quartz and feldspar (the most likely mineralogy of detrital grains) remain undigested (Selby and Creaser, 2003).

Both digestion methods are followed with osmium separation techniques outlined in the University of Maryland IGL Manual, March 23, 2004 Edition (See Appendix A). The rhenium separation from the inverse aqua regia also follows the anion exchange chemistry outlined in that manual. When employing the CrO_3 -H_2SO_4 solution, an extra step must be taken. Since Cr^{6+} complicates the anion exchange chromatography, the chromium is reduced to a 3+ valence state with the addition of sulfurous acid following Os separation as outlined in Selby and Creaser (2003). Once reduced, the Re-bearing solution can be passed through anion exchange columns (Appendix A). Once isolated, Os is dried onto a degassed platinum filament and isotopically analyzed using negative thermal ionization mass spectrometry (N-TIMS). Rhenium is taken up in 2% nitric acid and isotopically analyzed using solution introduction inductively coupled plasma mass spectrometry (ICP-MS).

2.4 $\delta^{13}C$ of TOC

Carbon isotopic measurements of total organic carbon (TOC) are made on acidified residues. Powdered samples are acidified repeatedly with 12N HCl and centrifuged in 15mL centrifuge tubes to remove all carbonate carbon. The samples are then rinsed with Milli-Q water and dried. Dry samples are accurately weighed out into tin cups. The loaded tin cups are combusted in a Eurovector elemental analyzer in-line with an Isoprime gas source mass spectrometer. The amount of residue required varied considerably. To generate a minimum peak height of ~2E-9 amps (necessary for precise results), between 2 and 12 mg of residue are required. The area is also used to determine the amount of carbon in the sample, providing a check on off-line TOC measurements. A urea standard run continuously throughout each analytical session is used to correct and reduce the data. The typical run sequence consisted of 10 samples (with one duplicate) bound with two urea standards on each end. Specific parameters of the EA-MS for carbon isotope and abundance analyses can be found in Appendix B. Uncertainties are then determined from the reproducibility of the bracketing urea measurements.

2.5 $\delta^{34}S$ of pyrite

Sulfur isotopic composition of pyrite in samples is determined using a chrome-reduction solution to isolate sulfides from bulk powders (as detailed in Canfield *et al*., 1986; Hsieh and Yang, 1989; Hsieh and Shieh, 1997) and an EA-MS to combust and measure the product Ag_2S. Approximately 0.5 g of powdered sample is weighed into a 50 mL beaker. The beaker is then placed in a plastic container adjacent to a second 50 mL beaker containing ~20 mL zinc acetate solution composed of 5 g of zinc acetate

dissolved in 432 mL Milli-Q water and 68 mL NaOH (50%w/w). The container is sealed and purged with nitrogen gas. Using a syringe, 15mL of 5N HCl are added to the 50mL beaker containing the powdered bulk sample. This dissolves any carbonate within the sample, helping to disseminate the matrix. The 5N HCl also releases any acid-volatile sulfur in the sample. Then, also using a syringe, 15mL of the chrome-reduction solution are added to the same beaker, reducing the mineral-bound chrome reducible sulfur to $H_2S(g)$. The $H_2S(g)$ reacts with the zinc acetate solution, precipitating ZnS. After 48 hours of reacting, the ZnS is rinsed with Milli-Q water and reacted with silver nitrate, converting the ZnS to Ag_2S. The sample is rinsed with ~3mL ammonium hydroxide to strip any excess metals. After a final Milli-Q rinse, the sample is dried and between 100 and 150μg of sample are weighed into a tin cup with an excess of vanadium pentoxide (V_2O_5) powder. The samples are analyzed in the elemental analyzer EA-MS. The V_2O_5 allows for a more complete combustion by adding an oxidant within the elemental analyzer. The NBS-127 standard bound runs (3 each on each side of 5 samples + 5 duplicates). Uncertainties are determined by reproducibility of NBS-127 sets that bookend sample measurements. If sulfide sulfur is deemed to be the overwhelming sulfur species, bulk sample powder (~1mg) can be placed into the tin vessel with vanadium pentoxide and run on the elemental analyzer to eliminate the time-consuming sulfide sulfur isolation chemistry. Specific EA-MS parameters for sulfur isotope and abundance measurements can be found in Appendix B.

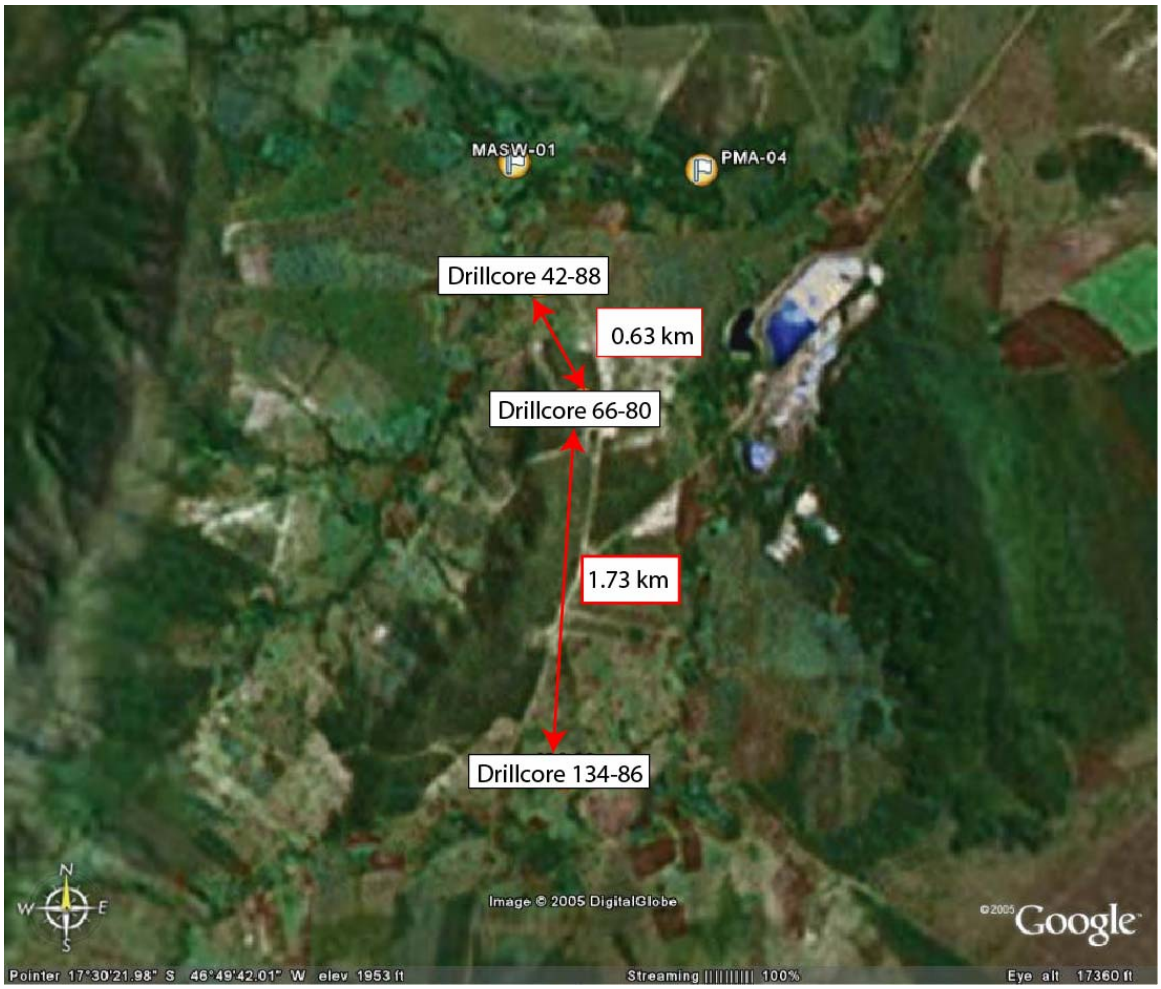

Figure 10. Google Earth map showing surface locations of the three drill holes' relative proximity to each other. Note the mine location nearly on top of drill hole 66-80.

2.6 Blanks

2.6.1 Osmium Blanks

Osmium concentrations within the sampled shales are generally low. To minimize uncertainties, total analytical blank contributions must be sufficiently below sample levels and isotopically well characterized. Initially, total blank contribution was as much as 8 picograms (pg) of osmium per digestion of sample using the inverse aqua regia digestion method. Since many reagents and processes are employed during osmium liberation and separation, troubleshooting was necessary to determine the source of this contaminant blank. To this extent, reagents used in the osmium separation chemistry were spiked and analyzed. In addition, labware used in the chemistry was also analyzed. During the digestion process, the glass carius tubes are etched, thus potentially adding Os to the blank. Therefore, different glasses used in carius tubes were powdered and analyzed. Pipette tips and centrifuge tubes used during the separation chemistry were soaked overnight in 6M HCl and then the HCl was tested to ensure no leaching of Os was taking place. Blanks were also run on processes including microdistillation and filament loading. The results are reported in Table 2. Concentrated hydrobromic acid contained only moderate levels of osmium. A second Teflon distillation reduced the hydrobromic acid contribution to negligible amounts.

It was discovered that the major source of osmium in the total analytical blank was nitric acid. Insofar as osmium is mobile in its oxidized form, it was supposed that nitric acid would be self cleaning (in that it oxidizes osmium). An unknown binding

mechanism, however, retains osmium within the acid. Quartz and Teflon distillations remove osmium from nitric acid, but not to the levels required. A second Teflon distillation also fails to lower Os blanks to acceptable levels. Other attempted methods of osmium mitigation also proved unsuccessful (Table 3). The acid was passed through an ion exchange column with the possibility of the osmium being sequestered into the resin, but no improvement was observed. An attempt to purify the acid of Os with carbon tetrachloride also failed. The theory is that the osmium within the acid is a polar compound (OsO_4) and would preferentially dissolve into the polar carbon tetrachloride. To ensure maintained control on the location of the osmium, the cleansing carbon tetrachloride as well as the cleansed nitric acid were tested to check mass balance with uncleansed nitric. The results in Fig. 11 show control on osmium mass balance. The acid was refluxed while oxygen gas bubbled through it to fully oxidize and mobilize the osmium. However, nitric acid and OsO_4 (the osmium species within the acid) have very similar boiling points, 122°C and 129°C, respectively. This makes it very difficult to remove osmium from the acid via distillation. Therefore, the acid was simply boiled while oxygen bubbled through it until its volume had been reduced by one-half. This process successfully removed enough osmium to reach negligible levels (less than 1pg per 10g solution; Table 2). Osmium was also successfully purged from the acid by adding 50mL of concentrated hydrogen peroxide to one liter of nitric acid. The resulting reaction violently degassed the acid of nitrous oxide which liberated the osmium. A second purge (followed by an hour on a hot plate to bring the acid back to normality) removed almost all osmium from the acid. This is the preferred method as it is the fastest and also involves little loss of nitric acid.

As nitric acid is the major contributor of osmium to total analytical blanks, it is only of concern with respect to the inverse aqua regia digestion method. In comparison, using chromic oxide saturated in 4N sulfuric acid as a digestion medium yields total analytical blanks of << 1pg/10g reagent, yielding total analytical blanks (of which 6mL of solution is used) to be under 1pg.

2.6.2 Rhenium Blanks

Chromic oxide-sulfuric acid digestions, however, introduced rhenium blank concerns not observed in inverse aqua regia digestion. Average rhenium blanks using inverse aqua regia are 4pg. Acids can be distilled (through both quartz and Teflon stills) to be cleansed of rhenium and other platinum group elements, thus the low levels in the inverse aqua regia. Rhenium cannot be removed, however, from chromic oxide. Rhenium is incorporated in chromium ores (chromite, for example) from which chromium oxide is manufactured. Any attempt to remove the rhenium through distillation would result in the reduction of the chromium to Cr^{3+} with no way of oxidizing it back to a +6 valence state. Due to these factors, initial Re blanks from chromic oxide-sulfuric acid oxidation were expectionally high (77-109pg).

Although chromic oxide can not be purified through distillation, a cerium based oxidizing medium can be. Ceric (IV) sulfate, like chromic oxide, is a strong oxidizer. Following Walker (1988), solid ammonium cerium nitrate is combined with sulfuric acid and the solution is distilled until no more liquid remains and is, presumably, stripped of rhenium. What remains is cleansed ceric (IV) sulfate. Following spiking, column chemistry and analyzing via ICP-MS, it was found the distilled ceric (IV) sulfate

contained 24pg/g of Re. Although this oxidative medium had lower blanks per gram of solution, using five grams alone could not completely oxidize sample powders, leading the total blank to be higher than the chromic oxide solution.

Since there is no method of removing rhenium from chromic oxide, low blank chromic oxide must be procured. Unfortunately, this requires ordering chromic oxide until a lot number with low enough initial concentrations of rhenium is found. The Fluka Company traditionally has a reputation for providing low Re-blank chromic oxide (Robert Creaser, pers. Comm.). Ordering new chromic oxide reduced total analytical rhenium blanks to ~19pg. All rhenium blanks can be seen in Table 4.

Table 2. Reagent and labware blanks for Os. *Indicates per 10g of reagent. **100mg of glass digested for analysis.

Reagents*:		
	$^{187}Os/^{188}Os$	Os (pg)
Milli-Q Water	0.226	0.061
Teflon Distilled Hydrochloric Acid	0.321	0.083
Carbon Tetrachloride	0.313	0.044
Teflon Distilled Hydrobromic Acid	0.132	0.74
2x Teflon Distilled Hydrobromic Acid	0.331	0.063
Teflon Distilled Nitric Acid	0.157	4.7
Labware:		
	$^{187}Os/^{188}Os$	Os (pg)
Microdistillation	0.148	0.054
Centrifuge Tube	0.153	0.037
Pipette Tips	0.138	0.62
Trembly Pyrex Body**	0.117	5.4
Trembly Pyrex Neck**	0.674	8.9
Trembly Prx/Hyd Body**	0.164	5.6
Trembly Prx/Hyd Neck**	0.198	6.2
Trembly Quartz Body**	0.198	5.6
Trembly Quartz Neck**	0.156	9.4
Chicago Pyrex Body**	0.199	5.7

Table 3. Os blanks for different nitric acids, the major contaminator to the total analytical blank. All levels are per 10g of nitric acid.

Nitric Acid:		
	$^{187}Os/^{188}Os$	Os (pg)
Reagent Grade Nitric Acid	0.192	12.0
Reagent Grade Nitric Acid dup	0.193	12.6
Qtz Distilled Nitric Acid	0.162	9.7
Refluxed Qtz Distilled Nitric Acid	0.170	7.9
Teflon Distilled Nitric Acid	0.157	4.7
Teflon Distilled Nitric Acid dup	0.160	5.6
Teflon Distilled Nitric Acid dup 2	0.165	6.6
2x Teflon Distilled Nitric Acid	0.156	7.1
2x Teflon Distilled Nitric Acid dup	0.156	7.0
Anion Exchange Nitric Acid	0.165	6.6
Boiled Nitric Acid	0.298	0.8
Boiled Nitric Acid dup	0.203	0.4
Purged Teflon Distilled Nitric Acid	0.192	1.9
Purged Teflon Distilled Nitric Acid dup	0.188	2.0
Purged Reagent Grade Nitric Acid	0.207	2.6
Purged Reagent Grade Nitric Acid dup	0.192	2.3
2x Purged Reagent Grade Nitric	0.334	0.84
2x Purged Reagent Grade Nitric dup	0.324	0.57

Teflon Distilled Nitric Acid		Cleansing Carbon Tetrachloride		Cleansed Teflon Distilled Nitric Acid
5.6pg	~	2.7pg	+	3.4pg

Figure 11. Mass balance of Os removed from nitric acid with carbon tetrachloride.

Table 4. Total analytical Re blanks using different digestive mediums.

	Re (pg)
Inverse Aqua Regia	1.77
Inverse Aqua Regia	1.47
Inverse Aqua Regia	9.52
CrO_3-H_2SO_4	76.9
CrO_3-H_2SO_4	78.8
CrO_3-H_2SO_4	93.9
CrO_3-H_2SO_4	109
Fluka CrO_3-H_2SO_4	21
Fluka CrO_3-H_2SO_4	20
Fluka CrO_3-H_2SO_4	16
Fluka CrO_3-H_2SO_4	18
Fluka CrO_3-H_2SO_5	18
Ce(IV)SO_4	24.8
Ce(IV)SO_4	23.7

Chapter 3: Results

3.1 Re-Os Results

Rhenium samples were measured using isotope-dilution inductively coupled plasma mass spectrometry, whereas osmium was measured using negative thermal ionization mass spectrometry. Reproducibility of rhenium mass spectrometry results was determined with repeat measurements of an intermediate standard, in this case a spiked solution of the Agpalilik iron meteorite. Over the two month measuring period average Agpalilik results of $^{185}Re/^{187}Re$ were 1.331 ± 0.002 (n=10; 2SDM). Long term osmium reproducibility was measured against an in-house osmium standard. Over the nine month measuring period $^{187}Os/^{188}Os$ measurements averaged 0.1140 ± 0.0003 (n=9; 2SDM) and $^{190}Os/^{192}Os$ measurements averaged 1.981 ± 0.002 (n=9; 2SDM).

Rhenium and osmium isotopic and concentration data can be seen in Tables 5-8. The Serra do Poço Verde Formation was analyzed in both drill hole 42-88 and drill hole 134-86. The Serra do Garrote and Lapa formations were sampled only from hole 134-86 where they were more extensively available. A general linear trend can be seen between rhenium and osmium concentrations (Fig. 12) for all samples in all cores. Samples treated with a chromic oxide-sulfuric acid solution (indicated with a "Cr" notation) from the Serra do Poço Verde Formation are not used in isochron regression. Following Selby and Creaser (2002), only 1 mL of the rhenium-bearing phase was reduced and analyzed, offering very poor rhenium recovery and calling into question the reliability of the data. Samples from the Serra do Garrote and Lapa formations had all 4 mL of the rhenium-

bearing phase reduced and analyzed, producing signal voltages two orders of magnitude higher.

The Serra do Garrote has rhenium and osmium concentrations ranging from ~1 to ~16 ppb and ~0.06 to about 0.6 ppb, respectively. Data for the Serra do Garrote Formation have an isochronous relationship. Figure 13 shows an isochron generated from five samples with four duplicates. The samples are within 1.5 stratigraphic meters of one another. The data set regress to give an age of 1353 ± 69 Ma (MSWD = 26). Due to the large uncertainty, however, little can be said about the initial osmium isotopic composition of the samples ($Os_i = 0.12 \pm 0.28$). Total analytical duplicates do not exactly repeat themselves, but do fall on the same isochron suggesting powder heterogeneity and closed system behavior. Sample 825.86Cr was measured six times, with $^{187}Re/^{188}Os$ ranging from 179.3 to 199.2 and $^{187}Os/^{188}Os$ values ranging from 4.202 to 4.496. All six samples do fall on a 1353 Ma isochron within analytical uncertainties. The Serra do Garrote samples also display similar model ages (1.27-1.43 Ga; Table 5). This will be explored further in the Discussion section.

Rhenium and osmium concentrations vary from drillcore to drillcore (Tables 6 and 7). Drillcore 42-88 contains ~0.30 to 0.85 ppb Re and ~0.027 to 0.055 ppb Os. Both Re and Os are much more highly concentrated in samples from drillcore 134-86 with ~1 to 23 ppb Re and ~0.04 to 0.7 ppb Os. The Serra do Poço Verde Formation was sampled in multiple drillcores. Data for samples from drillcore 134-86 that span 15 vertical meters define an errorchron with an age of 1063 ± 190 Ma (Fig. 14). The scatter about the line is attributed to the large stratigraphic range from which the five samples plus three duplicates were taken. Data for five samples from the same formation from

drillcore 42-88 defines an age of 1162 ± 350 Ma (Fig. 15). These five samples plus three duplicates span only 60 cm, but have very large errors associated with them due to the low concentrations of both rhenium and osmium. If these two data sets are assumed to be of coeval ages (based on stratigraphy and statistically identical isochron ages), then they may be combined into an isochron yielding an age of 1126 ± 47 Ma (Fig. 16). An additional sample set was measured for the Serra do Poço Verde formation from drillcore 134-86. Samples M1Cr-M5Cr (plus four duplicates) show an indistinguishable age, but with considerable scatter about an isochron (Fig. 17).

Samples from the Lapa Formation have Re and Os concentrations that range from ~0.1 to 0.3 ppb and ~0.03 to 0.05 ppb, respectively (Table 8). The Lapa Formation samples do not define an isochron (Fig. 18). The four samples from the Lapa Formation have similar osmium isotopic ratios, ranging from 1.59-1.709. Although the Lapa Formation is thick, only the lower 12 meters are composed of organic-rich shale, making sampling more difficult. The Lapa Formation also has the lowest concentrations of both rhenium and osmium of all samples measured.

Table 5. Re-Os data for the Serra do Garrote Fm. **Indicates samples used for isochron generation. Cr denotes sampled processed using chromic oxide.

	Re (ppb)	±	Os (ppb)	±	$^{187}Re/^{188}Os$	±	$^{187}Os/^{188}Os$	±	Age	Os_i	Model Age
Garrote 134-86											
824.37Cr**	16.02	0.07	0.5787	0.0008	222.5	1.0	5.257	0.003	1.4	0.19	1.37E+09
824.37Cr dup**	15.63	0.07	0.5682	0.0008	220.4	1.0	5.209	0.005	1.4	0.19	1.37E+09
824.37Cr A	15.27	0.03	0.5918	0.0012	204.1	0.6	5.055	0.009	1.4	0.40	1.43E+09
824.37Cr B	15.52	0.03	0.5953	0.0011	207.4	0.6	5.121	0.009	1.4	0.39	1.43E+09
824.42Cr**	11.56	0.06	0.3700	0.0006	274.9	1.6	6.468	0.006	1.4	0.20	1.37E+09
824.42Cr dup**	11.72	0.06	0.3568	0.0006	300.4	1.7	7.017	0.006	1.4	0.17	1.36E+09
824.42Cr A	11.21	0.02	0.3619	0.0008	270.6	0.9	6.366	0.015	1.4	0.20	1.37E+09
824.76Cr**	1.09	0.06	0.06041	0.00035	116.5	6.4	2.724	0.003	1.4	0.07	1.33E+09
824.76Cr dup**	1.04	0.06	0.0800	0.0004	76.5	4.4	1.844	0.002	1.4	0.10	1.34E+09
824.76Cr A	1.142	0.008	0.05888	0.00045	125.90	1.31	2.805	0.005	1.4	-0.07	1.27E+09
825.83Cr**	11.97	0.06	0.3553	0.0006	305.3	1.7	6.892	0.006	1.4	-0.07	1.32E+09
825.83Cr A	12.37	0.03	0.3603	0.0007	313.1	0.9	6.980	0.006	1.4	-0.16	1.30E+09
825.86Cr**	5.65	0.06	0.2234	0.0005	189.3	2.1	4.380	0.005	1.4	0.06	1.34E+09
825.86Cr dup	5.70	0.06	0.2234	0.0005	191.2	2.1	4.400	0.006	1.4	0.04	1.33E+09
825.86Cr A	5.384	0.014	0.2214	0.0005	179.3	0.6	4.202	0.002	1.4	0.11	1.35E+09
825.86Cr B	5.956	0.015	0.2260	0.0005	199.2	0.7	4.496	0.006	1.4	-0.05	1.30E+09
825.86Cr C	5.499	0.014	0.2225	0.0006	183.2	0.7	4.261	0.004	1.4	0.09	1.34E+09
825.86Cr D	5.801	0.014	0.2260	0.0005	192.2	0.7	4.384	0.003	1.4	0.00	1.32E+09

Table 6. Re-Os data for the Serra do Poço Verde Fm from drill hole 134-86. *Indicates sampled used in isochron generation. Rpt indicates the sample was processed once and analyzed twice as opposed to total analytical duplicates (dup).

	Re (ppb)	±	Os (ppb)	±	$^{187}Re/^{188}Os$	±	$^{187}Os/^{188}Os$	±	Age	Os_i	Model Age
Serra do Poço Verde											
134-86											
676.05*	3.498	0.007	0.1311	0.0018	195.1	2.7	4.159	0.004	1.1	0.46	1.23E+09
676.05dup*	3.485	0.007	0.1330	0.0018	194.3	2.6	4.323	0.006	1.1	0.64	1.28E+09
676.05Cr	3.65	0.04	0.1352	0.0003	202	2	4.361	0.006	1.1	0.54	1.25E+09
676.05Cr rpt	3.68	0.04	0.1352	0.0003	204	2	4.361	0.006	1.1	0.51	1.24E+09
677.40*	8.702	0.018	0.2478	0.0018	292.0	2.2	5.744	0.005	1.1	0.21	1.15E+09
677.40dup*	8.030	0.017	0.2307	0.0018	302.8	2.4	6.365	0.009	1.1	0.63	1.23E+09
677.40Cr	8.023	0.043	0.2288	0.0004	313.4	1.8	6.686	0.006	1.1	0.75	1.24E+09
677.40Cr rpt	8.024	0.043	0.2288	0.0004	313.4	1.8	6.686	0.006	1.1	0.75	1.24E+09
680.78*	6.137	0.013	0.2161	0.0018	214.9	1.9	4.539	0.005	1.1	0.47	1.22E+09
680.78dup*	5.871	0.012	0.2150	0.0018	204.6	1.7	4.417	0.005	1.1	0.54	1.25E+09
680.78Cr	6.233	0.042	0.2156	0.0004	220.8	1.5	4.617	0.004	1.1	0.44	1.21E+09
680.78Cr rpt	6.329	0.042	0.2156	0.0004	224.2	1.5	4.617	0.004	1.1	0.37	1.19E+09
683.60*	4.070	0.009	0.1289	0.0018	258.6	3.6	5.581	0.006	1.1	0.68	1.25E+09
683.60Cr	4.737	0.041	0.1275	0.0003	316.0	2.8	6.004	0.008	1.1	0.02	1.11E+09
683.60Cr rpt	4.787	0.041	0.1275	0.0003	319.4	2.8	6.004	0.008	1.1	-0.04	1.10E+09
691.23*	6.570	0.014	0.1866	0.0018	297.9	2.9	5.993	0.004	1.1	0.35	1.17E+09
M1Cr	2.068	0.009	0.04564	0.00044	464.9	4.9	8.912	0.008	1.1	0.11	1.12E+09
M1Crdup	2.187	0.009	0.0442	0.0004	505.1	2.5	8.916	0.026	1.1	-0.65	1.04E+09
M2Cr	1.253	0.008	0.04780	0.00045	200.0	2.3	4.652	0.005	1.1	0.86	1.35E+09
M3Cr	23.58	0.05	0.765	0.001	240.8	0.6	4.899	0.004	1.1	0.34	1.18E+09
M3Crdup	23.66	0.05	0.7429	0.002	249.7	1.1	4.941	0.014	1.1	0.21	1.15E+09
M4Cr	1.022	0.008	0.03913	0.00044	188.4	2.6	3.987	0.006	1.1	0.42	1.22E+09
M4Crdup	1.052	0.008	0.03572	0.00044	217.1	3.3	4.282	0.008	1.1	0.17	1.14E+09
M5Cr	3.509	0.011	0.0993	0.0005	349.2	2.0	8.242	0.016	1.1	1.63	1.38E+09
M5Crdup	3.612	0.011	0.09823	0.00048	358.5	1.5	8.058	0.017	1.1	1.27	1.31E+09

Table 7. Re-Os data for the Serra do Poço Verde Fm. from drill hole 42-88. *Indicate samples used for isochron generation.

	Re (ppb)	±	Os (ppb)	±	$^{187}Re/^{188}Os$	±	$^{187}Os/^{188}Os$	±	Age	Os_i	Model Age
Serra do Poço Verde 42-88											
803.89*	0.4346	0.0017	0.0316	0.0018	80.8	4.5	1.86	0.01	1.1	0.33	1.28E+09
803.89dup*	0.3600	0.0016	0.0315	0.0018	67.3	3.8	1.88	0.01	1.1	0.60	1.55E+09
803.89Cr	0.38	0.04	0.03240	0.00023	53	9	1.787	0.002	1.1	0.77	1.85E+09
804.00*	0.6898	0.0020	0.0427	0.0017	99.9	4.1	2.352	0.003	1.1	0.46	1.33E+09
804.43*	0.3342	0.0017	0.0316	0.0018	59.6	3.4	1.46	0.00	1.1	0.34	1.34E+09
804.43dup*	0.3032	0.0016	0.0268	0.0018	65.9	4.4	1.79	0.00	1.1	0.54	1.50E+09
804.43Cr	0.28	0.04	0.05296	0.00024	60	4	1.759	0.002	1.1	0.61	1.61E+09
804.48*	0.8576	0.0023	0.0508	0.0018	106.5	3.8	2.549	0.010	1.1	0.53	1.35E+09
804.48dup*	0.8309	0.0022	0.063	0.002	77.5	2.2	1.911	0.009	1.1	0.44	1.37E+09
804.48Cr	0.835	0.040	0.03464	0.00023	98.8	7.3	2.444	0.002	1.1	0.57	1.40E+09
804.50*	0.3865	0.0017	0.0335	0.0018	67.6	3.6	1.82	0.01	1.1	0.54	1.50E+09
804.50Cr	0.29	0.04	0.05542	0.00024	50	4	1.800	0.002	1.1	0.86	2.00E+09

Table 8. Re Os data for the Lapa Formation. Note the low concentrations of both Re and Os.

	Re (ppb)	±	Os (ppb)	±	$^{187}Re/^{188}Os$	±	$^{187}Os/^{188}Os$	±	Age	Os_i	Model Age
Lapa 134-86											
L1Cr	0.322	0.008	0.03504	0.00044	53.34	1.19	1.709	0.003	Unknown	Unknown	1.77E+09
L3Cr	0.288	0.008	0.03338	0.00044	50.73	1.53	1.838	0.007	Unknown	Unknown	2.01E+09
L4Cr	0.138	0.008	0.0261	0.0004	30.4	1.8	1.59	0.01	Unknown	Unknown	2.86E+09
L5Cr	0.366	0.008	0.05230	0.00046	39.05	0.92	1.358	0.006	Unknown	Unknown	1.88E+09

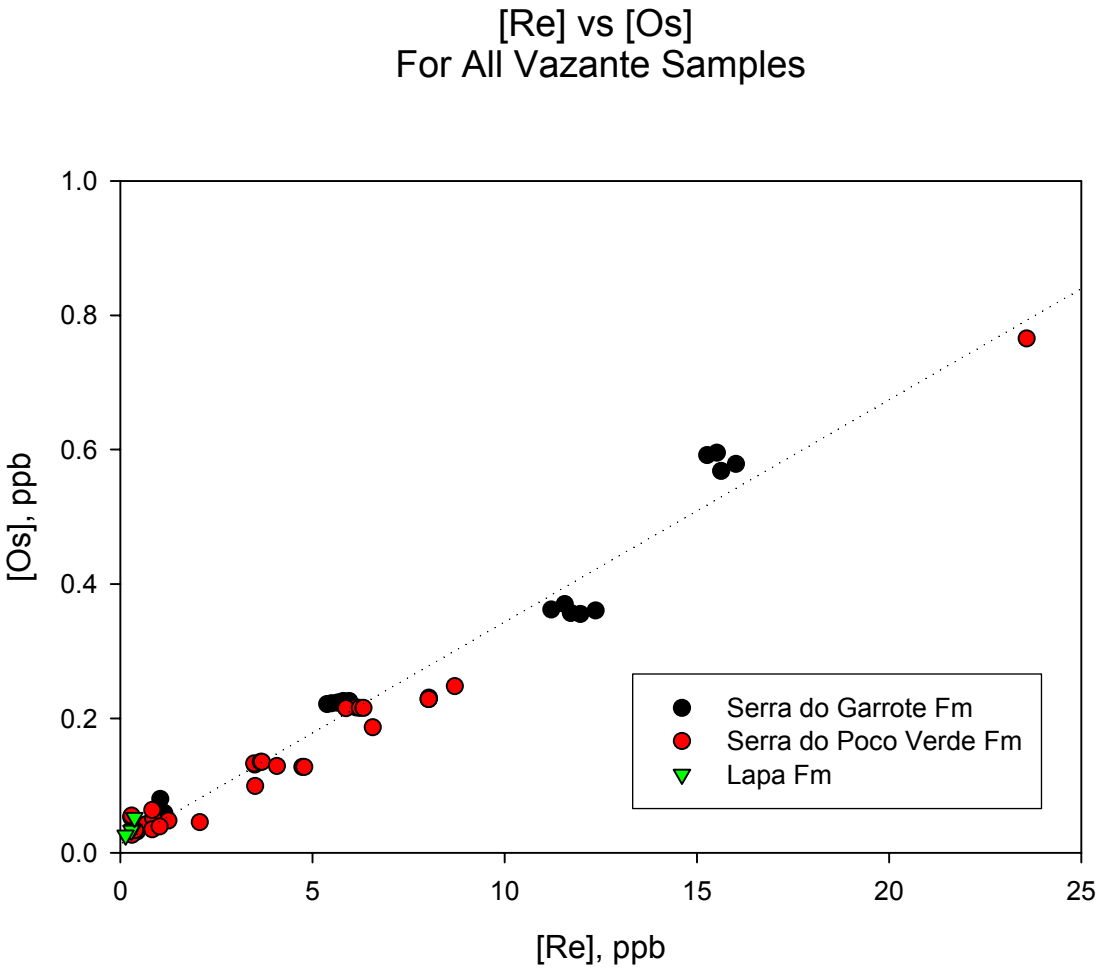

Figure 12. A general linear relationship of [Re] vs [Os] for all samples in the studied Vazante Group cores.

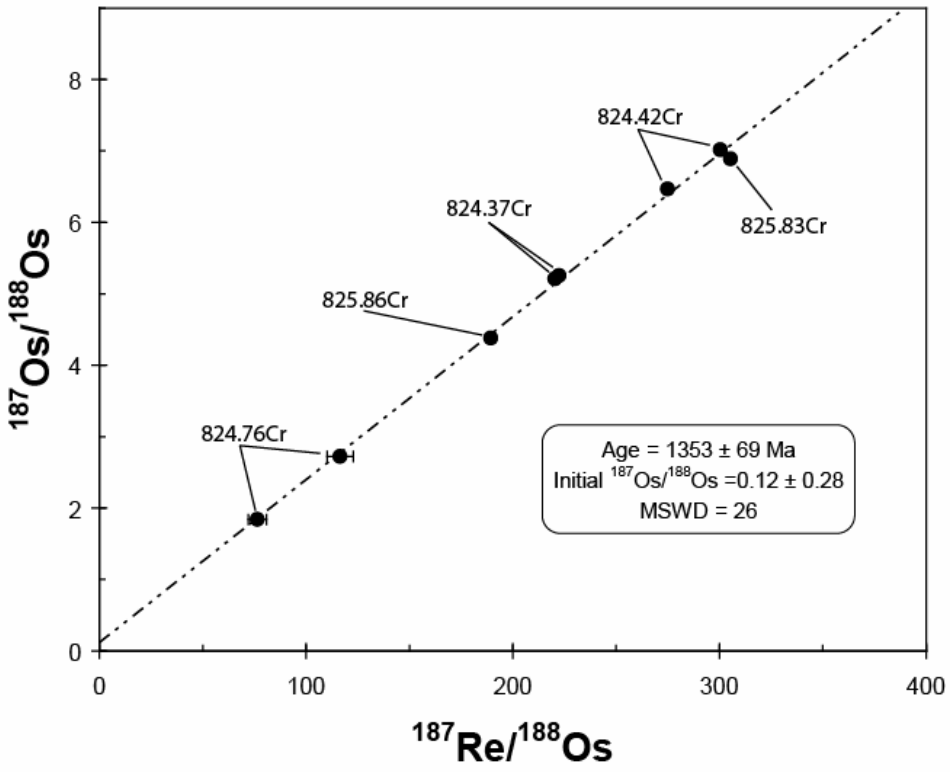

Figure 13. Isochron for the Serra do Garrote Fm from drillcore 134-86. Samples span less than 1.5 meters.

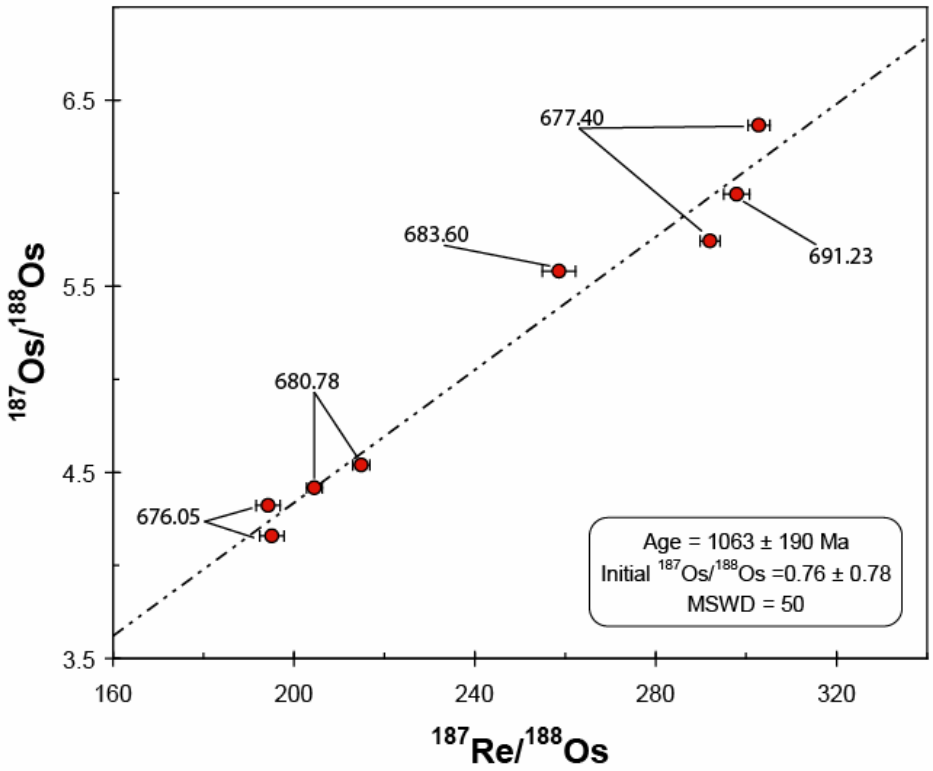

Figure 14. Isochron for Serra do Poço Verde Fm. from drill hole 134-86. Samples span 15 vertical meters.

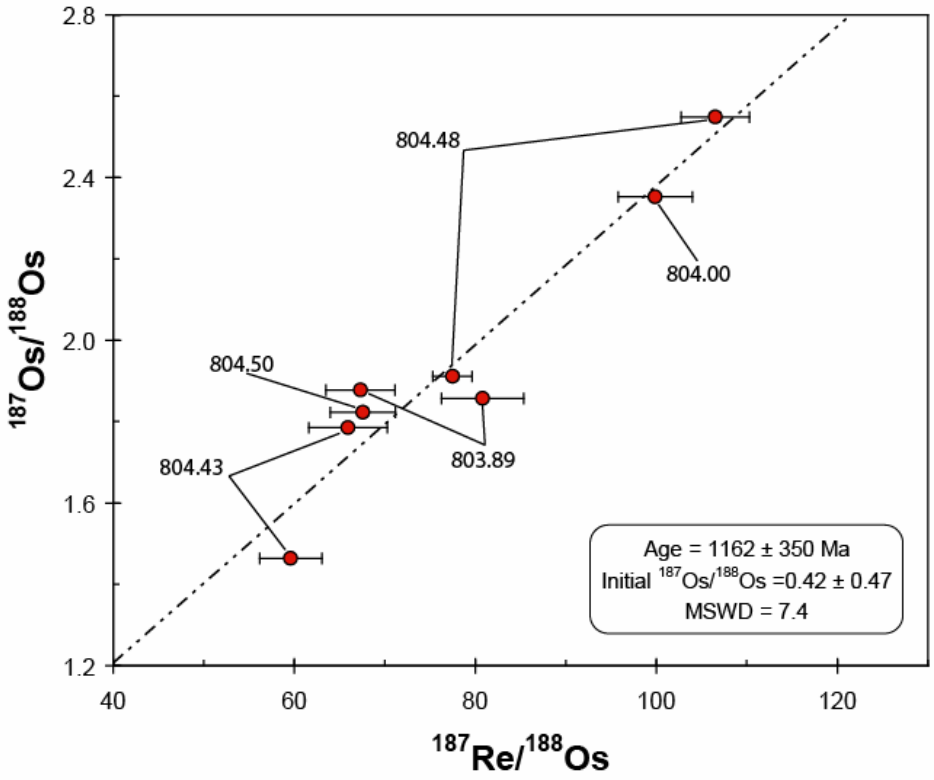

Figure 15. Isochron for the Serra do Poço Verde Fm. from drill hole 42-88. Samples span 60 cm.

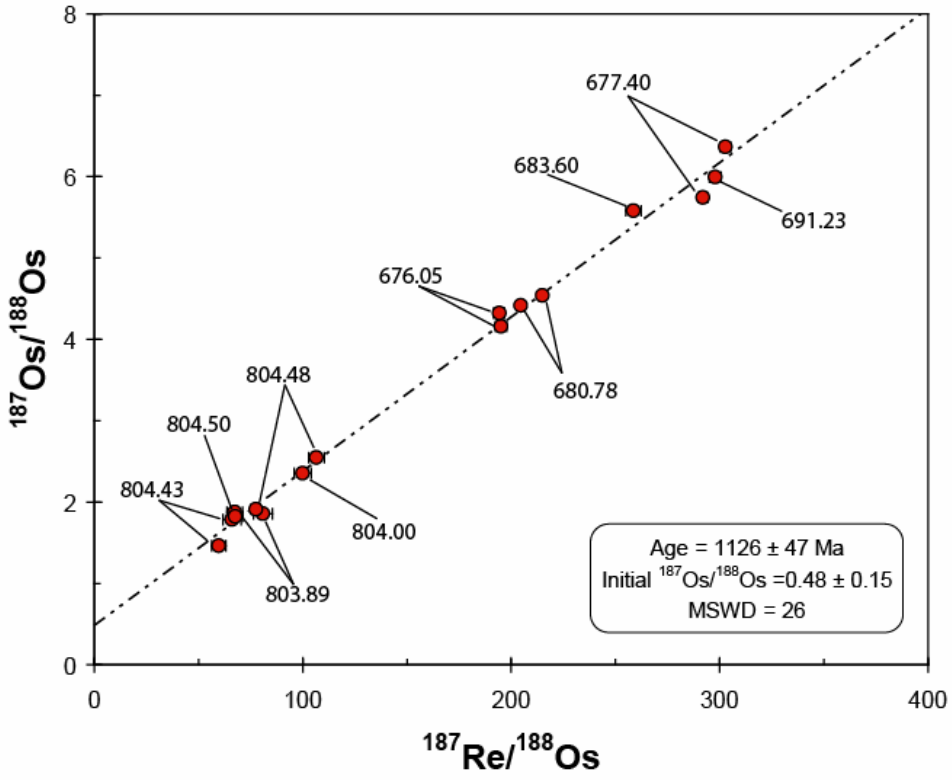

Figure 16. Combined isochron for the Serra do Poço Verde Fm. Samples include those from both Figures 14 and 15.

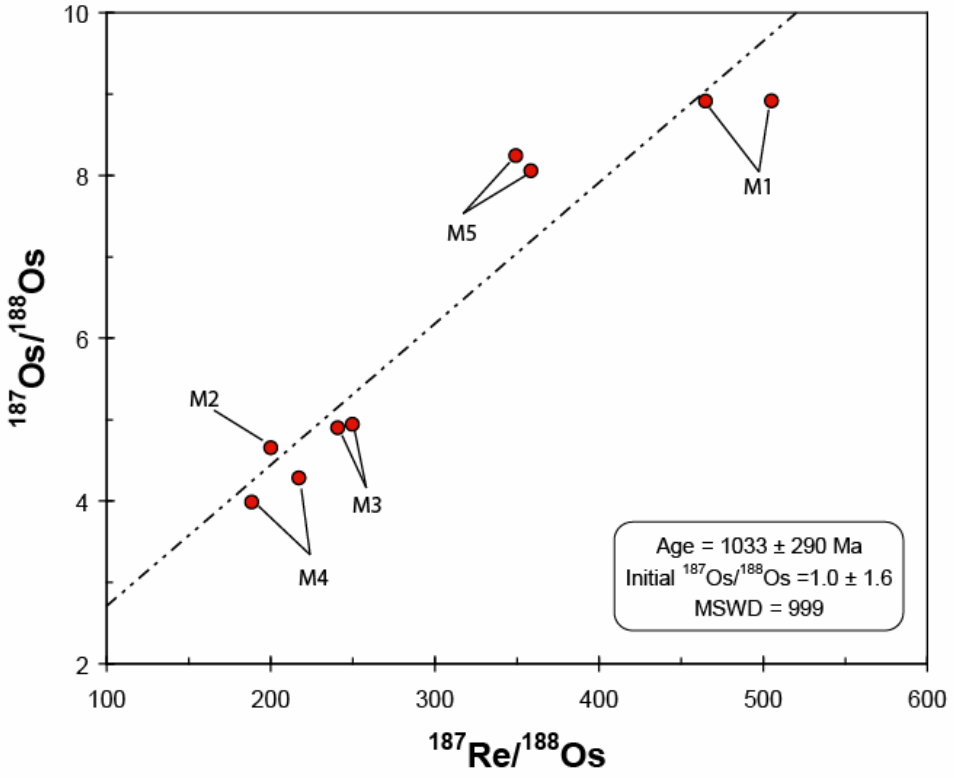

Figure 17. Isochron for samples M1-M5 with duplicates for the Serra do Poço Verde Fm. Samples are within 1.5 stratigraphic meters. Scatter appears to indicate open-system behavior.

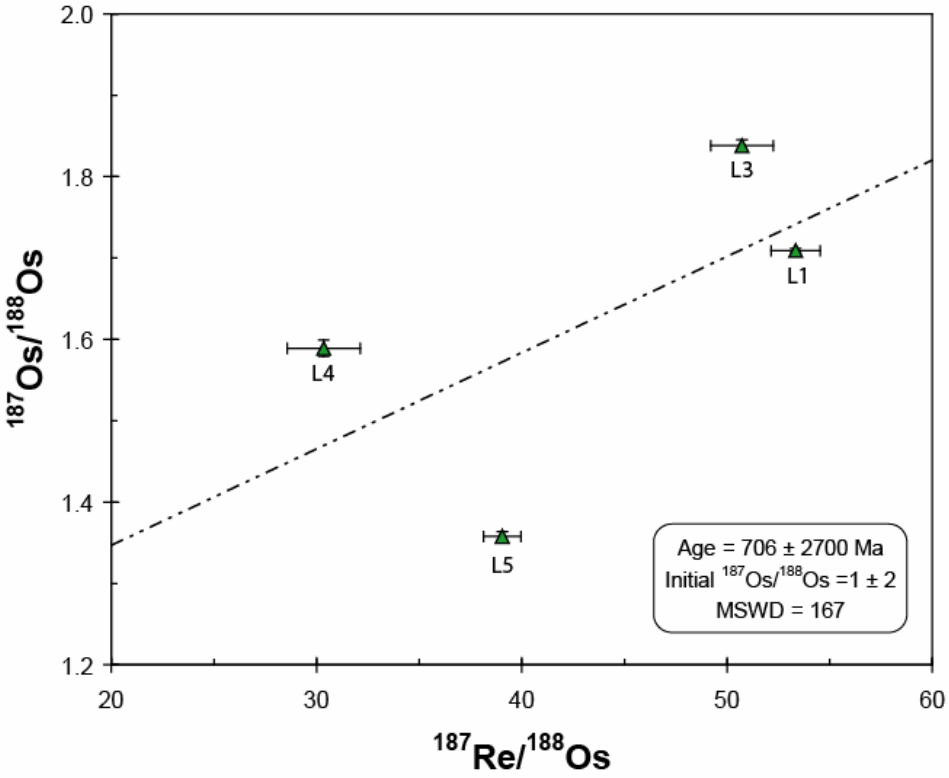

Figure 18. Regression for the Lapa Formation. Note the absence of a tight correlation and small spread in isotopic compositions of the four samples.

3.2 Carbon and Sulfur Results

Carbon and sulfur isotopic data are acquired using EA combustion techniques outlined in the Methods. Uncertainties were calculated using reproducibilities of standards which bookend run sequesnces.

Total organic carbon (TOC) abundances and the carbon isotopic composition of the organic carbon were measured in the synglacial Serra do Poço Verde Formation in three drill cores (Tables 9-11). Samples from drillcore 66-80 contain up to ~3.5 wt % TOC. The isotopic composition is generally constant with depth (from -25 to -27‰) save one pronounced positive excursion up to approximately -23‰ (Fig. 19). Drill hole 42-88 has relatively low organic preservation (<0.5 wt %) throughout the upper and lower section of the Serra do Poço Verde, but significantly higher preservation from ~820-800 meters of depth, reaching to over 3.0 wt % (Fig. 20). Isotopically, the organic carbon shows little variation with depth, with most samples falling within an expected range of -28 to -24‰. Drillcore 134-86 contains the highest preservation of organic carbon, upwards of 4.0 wt % (Fig. 21). A more comprehensive focus was taken with this drillcore.

Carbon and sulfur isotopic data for drillcore 134-86 can be seen in tables 11-13. Organic carbon abundances and isotopic composition of the Serra do Garrote Formation range from <1 to ~3.4 wt.% and ~-25 to -30‰, respectively (Fig. 21). Within the Serra do Poço Verde Formation, organic carbon data range from ~ -32 to -22‰. Sulfide sulfur isotopes also vary widely from ~ -20 to +25‰. Beginning at the base and moving up section, the carbon and sulfur isotopes vary inversely to each other; that is, there is an anti-correlation (Fig. 21). In the overlying Lapa Formation organic carbon isotopes

stabilize around -26 to -22‰ while sulfide sulfur isotopes begin very heavy at upwards of +30‰ before falling to values ranging from +5 to +20‰ up section (Fig. 21).

Table 9. Organic carbon abundance and isotopic composition for the Serra do Poço Verde Fm. in drill hole 66-80.

Drill Hole 66-80

Depth (m)	TOC (Wt %)	±	$\delta^{13}C$	±
679.64	0.254	0.024	-25.78	0.06
681.70	0.275	0.026	-25.37	0.17
683.41	0.239	0.023	-25.27	0.05
685.00	0.179	0.017	-25.41	0.17
686.06	1.74	0.16	-26.07	0.19
686.78	2.26	0.21	-25.86	0.19
688.37	1.29	0.12	-26.26	0.20
690.15	0.388	0.037	-25.8	0.3
692.12	0.999	0.094	-26.40	0.19
693.91	1.03	0.10	-25.52	0.19
694.33	0.958	0.091	-23.3	0.3
694.47	1.10	0.10	-23.28	0.18
695.01	1.45	0.14	-24.48	0.19
695.67	1.05	0.10	-26.29	0.11
697.21	0.904	0.085	-26.12	0.11
699.11	0.723	0.068	-26.40	0.11
701.04	1.28	0.12	-26.10	0.20
702.43	3.45	0.33	-26.55	0.13
705.17	1.28	0.12	-25.87	0.20
707.15	0.704	0.067	-26.59	0.20
708.44	0.424	0.040	-26.59	0.11
710.55	0.542	0.051	-26.38	0.06

Table 10. Organic carbon abundance and isotopic data for the Serra do Poço Verde Fm. from drill hole 42-88, nd = not determined.

Drill Hole 42-88

Depth (m)	TOC (Wt %)	±	$\delta^{13}C$	±
749.13	0.404	0.038	-28.3	0.3
752.46	0.156	0.015	-25.93	0.10
756.25	0.333	0.031	-26.0	0.3
759.60	0.0797	0.0075	-26.34	0.11
764.52	0.0788	0.0075	-26.4	0.3
769.81	0.0440	0.0042	-26.3	0.3
774.24	0.0336	0.0032	-26.0	0.3
779.17	0.0484	0.0046	-26.05	0.10
783.58	0.0827	0.0078	-25.64	0.10
788.26	0.314	0.030	-26.59	0.11
793.77	0.0226	0.0021	-22.36	0.10
799.18	1.98	0.19	-29.09	0.23
799.32	1.53	0.14	-25.19	0.18
799.43	1.72	0.16	-25.15	0.20
800.04	0.0410	0.0039	-24.12	0.05
800.21	0.142	0.013	-23.64	0.05
800.66	1.31	0.12	-25.14	0.20
801.42	1.05	0.10	-25.27	0.11
802.72	1.69	0.16	-25.57	0.20
803.91	0.890	0.084	-25.38	0.11
804.52	1.79	0.17	-25.05	0.20
804.74	0.675	0.064	-25.23	0.06
806.14	2.45	0.23	-26.56	0.07
807.80	0.431	0.041	-25.58	0.11
808.44	0.750	0.071	-25.98	0.19
809.18	0.831	0.079	-25.41	0.11
810.20	0.420	0.040	-25.89	0.06
810.60	1.90	0.18	-26.26	0.21
811.84	3.03	0.29	-25.84	0.13
813.11	1.91	0.18	-26.30	0.21
814.26	1.82	0.17	-25.21	0.20
814.56	0.479	0.045	-25.78	0.11
815.15	0.643	0.061	nd	nd
817.00	0.507	0.048	-25.89	0.19
818.10	2.09	0.20	-26.99	0.07
818.33	1.06	0.10	-26.86	0.12
820.27	0.0802	0.0076	-24.96	0.05
825.33	0.221	0.021	-21.54	0.17
830.07	0.0650	0.0061	-20.17	0.04
835.45	0.282	0.027	-23.07	0.16

Table 11. Total organic Carbon (TOC) abundance and isotopic composition and sulfide sulfur composition of the Serra do Poço Verde Fm. from drillhole 134-86, nd = not determined.

Serra do Poço Verde Fm. Drill Hole 134-86

Depth (m)	TOC (Wt %)	±	$\delta^{13}C$	±	$\delta^{34}S$	±
606.80	nd	nd	nd	nd	23.48	0.19
607.78	nd	nd	nd	nd	20.33	0.96
607.84	nd	nd	nd	nd	21.38	1.01
608.70	nd	nd	nd	nd	nd	nd
610.52	nd	nd	nd	nd	8.77	0.27
611.58	nd	nd	nd	nd	-1.97	0.06
612.23	1.57	0.15	-25.56	0.07	14.72	0.12
613.13	1.65	0.16	-25.76	0.07	23.66	0.19
614.27	0.543	0.051	-25.74	0.06	19.90	0.19
616.20	0.596	0.056	-21.82	0.05	nd	nd
619.69	0.021	0.002	-21.08	0.28	nd	nd
620.09	0.900	0.085	-28.99	0.07	-1.89	0.02
622.46	1.33	0.13	-29.90	0.22	3.29	0.03
624.86	1.38	0.13	-30.04	0.22	-1.83	0.02
627.72	0.484	0.046	-24.71	0.17	3.20	0.03
628.43	0.578	0.055	-26.75	0.07	nd	nd
638.17	3.43	0.32	-23.20	0.12	-5.84	0.06
638.69	0.431	0.041	-25.15	0.34	-13.03	0.14
639.38	1.12	0.11	-26.11	0.11	-2.46	0.03
640.89	0.364	0.034	-25.14	0.34	nd	nd
642.05	2.82	0.27	-27.07	0.07	1.10	0.01
644.05	4.04	0.38	-26.43	0.13	nd	nd
648.61	0.382	0.036	-23.34	0.31	nd	nd
649.32	0.191	0.018	-22.57	0.05	1.45	nd
651.31	0.214	0.020	-22.56	0.15	nd	nd
655.02	0.560	0.053	-24.48	0.06	-4.82	0.15
658.16	1.27	0.12	-27.51	0.22	5.70	0.27
662.25	3.26	0.31	-28.85	0.14	5.25	0.17
667.29	0.672	0.064	-28.24	0.07	nd	nd
668.73	1.60	0.15	-29.07	0.08	5.25	0.17
674.09	1.19	0.11	-29.03	0.21	15.61	0.52
676.12	2.19	0.21	-29.73	0.22	9.88	0.33
677.55	2.06	0.20	-29.37	0.08	7.32	0.35
680.82	1.52	0.14	nd	nd	8.45	0.40
683.69	2.42	0.23	-30.06	0.08	nd	nd
688.14	1.29	0.12	-29.54	0.22	8.26	0.39
691.32	3.82	0.36	-29.37	0.15	3.15	0.15
696.27	1.91	0.18	nd	nd	4.01	0.12

Table 12. Total organic carbon (TOC) abundance and isotopic composition and sulfide sulfur composition of the Serra do Garrote Fm. from drillhole 134-86, nd = not determined.

Serra do Garrote Fm. Drill Hole 134-86

Depth (m)	TOC (Wt %)	±	$\delta^{13}C$	±
822.93	2.39	0.19	-30.27	0.17
823.45	2.73	0.22	-28.95	0.16
824.35	2.07	0.17	-28.74	0.16
824.73	1.75	0.14	-29.74	0.16
825.83	1.61	0.13	-30.00	0.16
827.32	1.49	0.12	-29.96	0.07
827.47	2.01	0.16	-29.62	0.16
828.75	1.03	0.08	-29.39	0.07
829.32	0.832	0.067	-29.08	0.07
831.00	0.906	0.073	-29.31	0.07
831.25	0.312	0.025	-28.38	0.07
832.83	0.585	0.047	-28.92	0.07
833.73	0.643	0.051	-28.63	0.07
833.88	0.234	0.019	-25.32	0.06
835.29	0.518	0.041	-28.64	0.07
836.36	0.375	0.030	-28.95	0.07
837.00	0.806	0.064	-29.31	0.14
838.87	0.845	0.068	-28.75	0.14
838.92	0.234	0.019	-28.37	0.13
839.58	0.195	0.016	-28.31	0.13
841.35	0.208	0.017	-28.14	0.14
841.55	0.260	0.021	-28.85	0.14
844.00	0.494	0.040	-29.80	0.14
844.79	0.455	0.036	-30.04	0.14
845.29	1.19	0.10	-30.74	0.13
846.53	0.844	0.068	-30.37	0.14
847.69	3.42	0.27	-29.90	0.07
848.00	2.62	0.21	-29.76	0.07
848.90	2.16	0.17	-29.73	0.07
850.12	2.40	0.19	-29.75	0.07
851.15	2.53	0.20	-30.12	0.07
850.12	2.40	0.19	-29.75	0.07
851.15	2.53	0.20	-30.12	0.07

Table 13. Total organic carbon (TOC) abundance and isotopic composition and sulfide sulfur composition of the Lapa Fm. from drillhole 134-86, nd = not determined.

Lapa Fm. Drill Hole 134-86

Depth (m)	TOC (Wt %)	±	$\delta^{13}C$	±	$\delta^{34}S$	±
560.70	0.161	0.011	-25.83	0.09		
561.82	0.200	0.014	-24.66	0.09	11.91	0.27
565.40	0.220	0.015	-26.02	0.09	19.58	0.35
567.83	0.100	0.007	nd	nd	11.67	0.35
572.64	0.230	0.016	-24.37	0.09	17.59	0.18
575.60	0.190	0.013	-24.80	0.09	9.62	0.18
576.93	nd	nd	nd	nd	20.69	0.35
577.92	0.080	0.006	-24.48	0.09	27.09	0.24
579.27	nd	nd	-25.23	0.09	nd	nd
580.83	0.070	0.005	-25.83	0.19	nd	nd
582.74	0.100	0.007	-25.42	0.09	20.93	0.18
585.00	0.240	0.017	-24.66	0.19	15.49	0.35
585.60	0.210	0.015	-24.80	0.19	16.50	0.18
585.80	0.120	0.008	-25.40	0.27	14.48	nd
586.20	0.220	0.015	-23.24	0.33	19.99	0.27
587.84	1.47	0.10	-25.06	0.35	26.40	nd
589.90	1.45	0.10	-25.66	0.36	30.07	0.27
590.50	1.50	0.11	-25.42	0.19	29.13	0.27
591.34	3.73	0.26	-24.84	0.15	nd	nd
592.23	1.00	0.07	-25.23	0.19	30.10	0.27
593.20	0.440	0.031	-24.48	0.19	34.69	0.24
593.28	0.650	0.046	nd	nd	35.52	0.27
593.47	0.460	0.032	-24.37	0.19	27.02	0.27
594.04	1.68	0.12	-24.85	0.26	28.81	0.24
595.42	1.12	0.08	-25.18	0.27	26.00	0.27
596.20	0.440	0.031	-24.88	0.26	26.85	0.27
596.33	nd	nd	-25.32	0.27	27.18	0.24
596.85	nd	nd	-25.79	0.36	28.70	0.24
597.43	0.130	0.009	nd	nd	28.86	0.27
598.10	0.150	0.011	-26.02	0.19	19.52	0.27

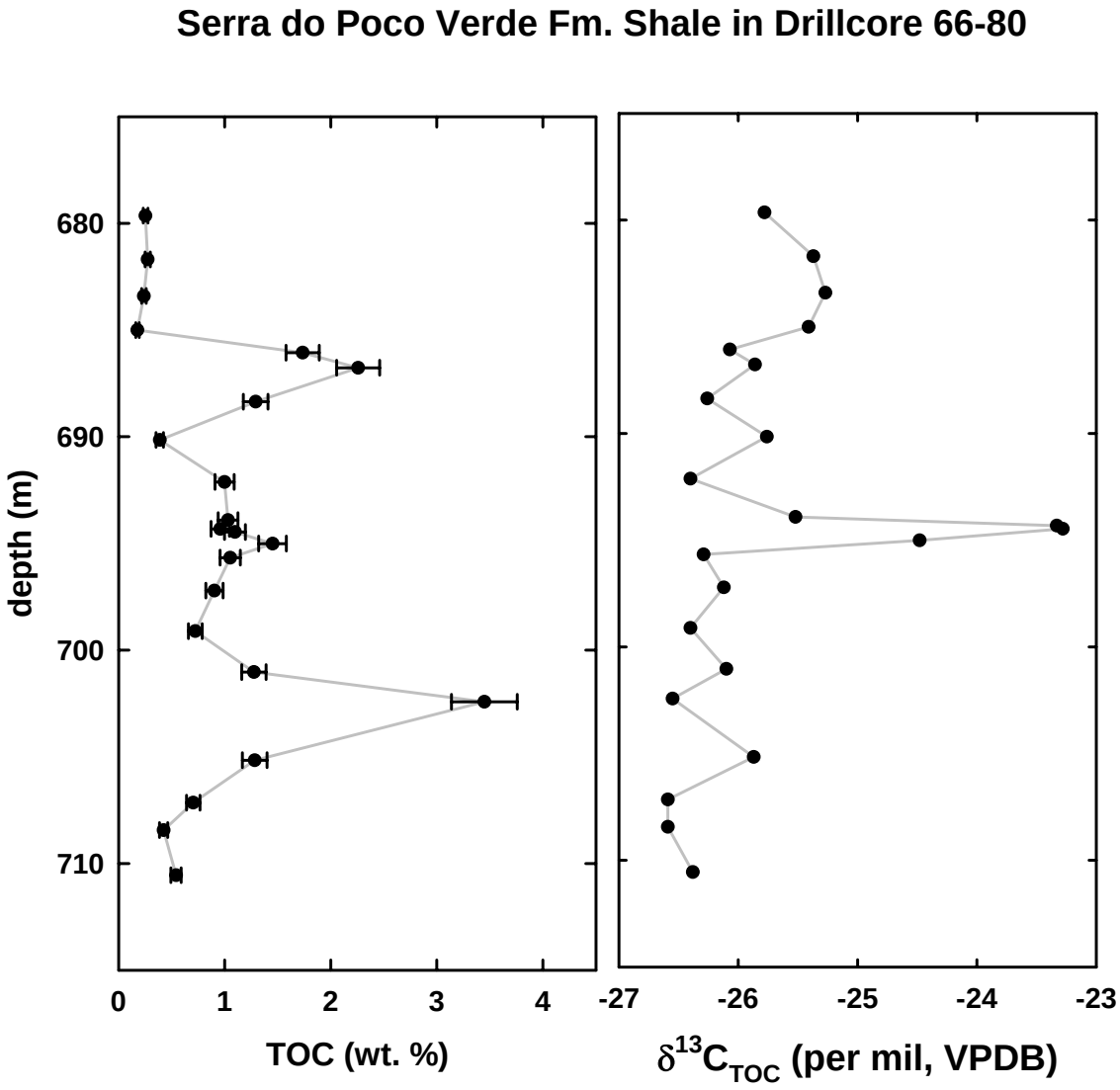

Figure 19. Total organic carbon abundance and isotopic composition of the Serra do Poço Verde Fm. from drill hole 66-80.

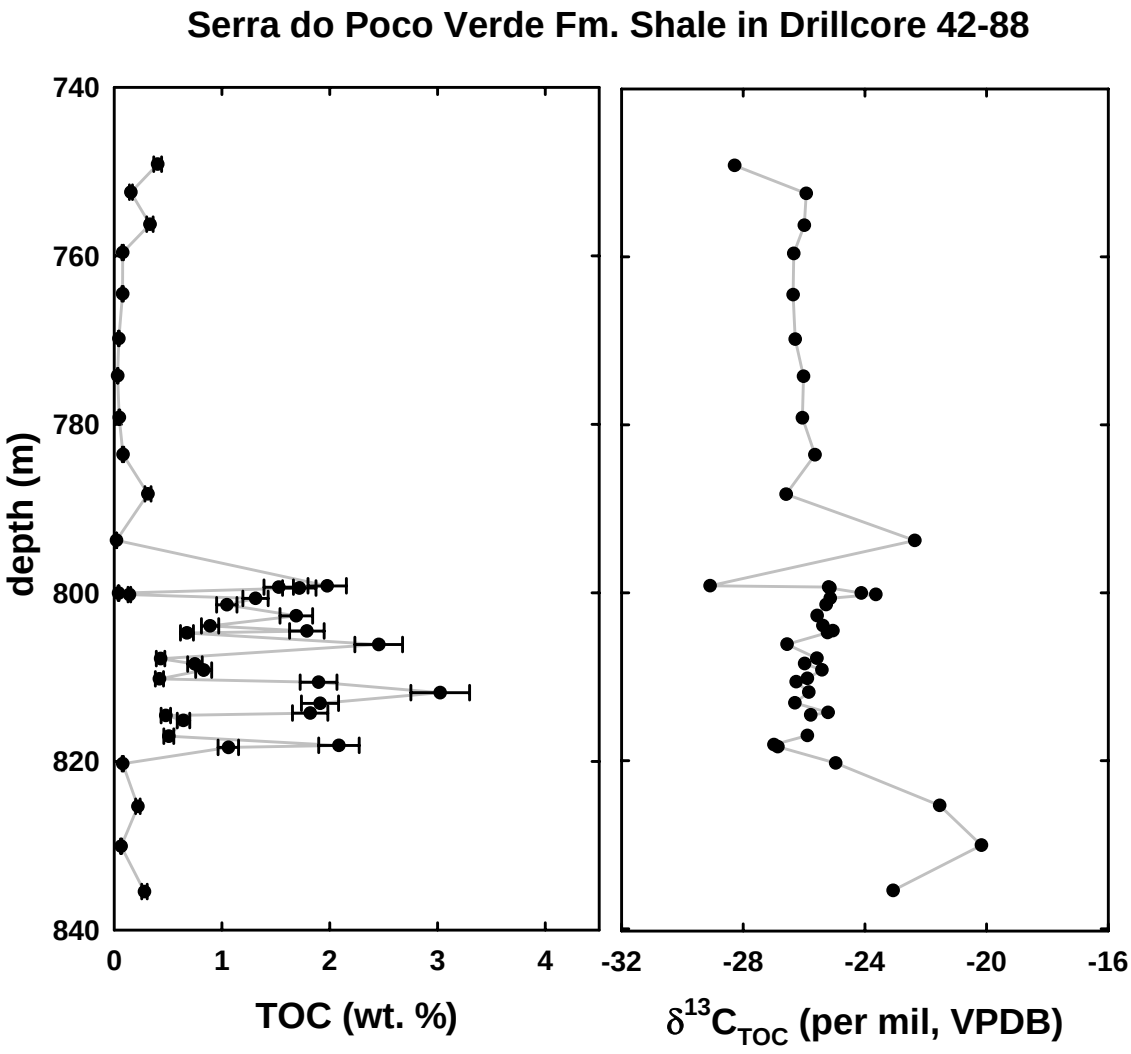

Figure 20. Total organic carbon abundance and isotopic composition of the Serra do Poço Verde Fm. from drill hole 42-88.

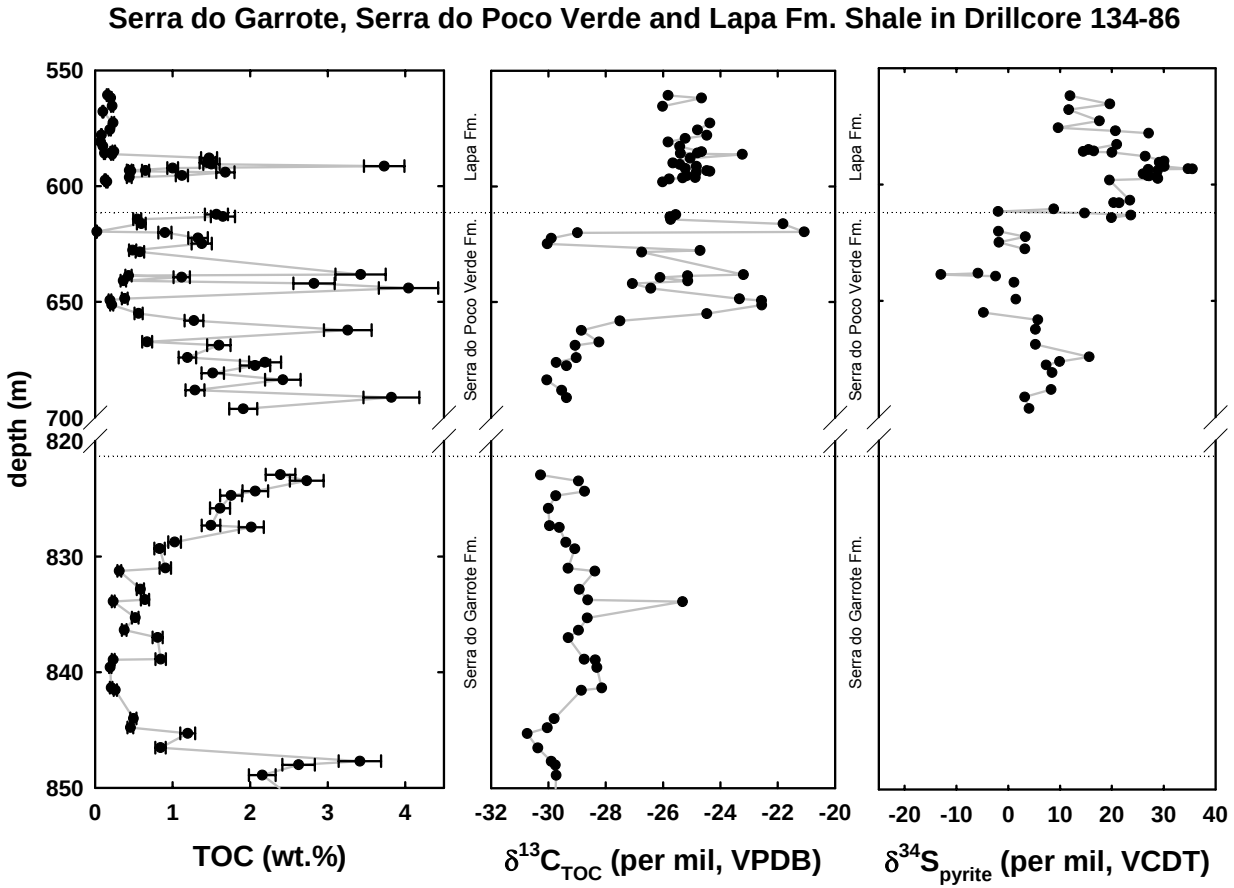

Figure 21. Abundance of organic carbon, isotopic composition of organic carbon and isotopic composition of sulfide sulfur from the Serra do Garrote, Serra do Poço Verde and Lapa Formations. Uncertainties in isotopic data are smaller than data point.

Chapter 4: Discussion

4.1 Depositional and Tectonic Setting

The rhenium-osmium ages place the Vazante Group in a significantly older context than suggested by some previous studies. The dates of 1353 ± 69 and 1126 ± 47 Ma are interpreted to be depositional ages for the Serra do Garrote and Serra do Poço Verde formations, respectively, with scatter about the isochron due to subtle changes in intial osmium isotopic values and some degree of open-system behavior. Several recent papers have placed the Vazante Group strata within a window of time between 800 and 700 Ma (i.e. Azmy *et al.*, 2001; Olcott *et al.*, 2005; Azmy *et al*., 2006). For example, using isotope stratigraphy, Azmy and others (2001) sought to correlate the Vazante with other globally distributed Neoproterozoic formations. Carbon isotopes exhibit a negative excursion of roughly 4‰ (from +2 to -2) in the Serra do Poço Verde Formation (a trend, albeit smaller in scale than seen elsewhere, common in the "Sturtian" glacial phase of ~800 to 650 Ma) as well as a single low $^{87}Sr/^{86}Sr$ value of 0.70614 in the Lapa Formation, a value consistent with other "Sturtian" aged rocks. Carbon isotopic trends are open to multiple interpretations, and can not "fingerprint" an exact geologic time or event. In addition the baseline for Precambrian chemostratigraphy is believed by some not to be sufficiently refined to allow for direct age assignment (*cf*. Babinki *et al*., 2005). Oceanic strontium isotopes progress to higher values through Neoproterozoic time, but the increase is not linear; there is apparent variation which makes the use of strontium isotopic values as time markers problematic. Nonetheless, Olcott and others (2005) investigated biomarkers in the Serra do Poço Verde Formation and interpreted them in

the context of a Sturtian global glaciation. The biomarkers found in that study include those indicative of cyanobacteria, green sulfur bacteria, aerobic eukaryotes and aerobic methanotrophs. These bacteria are known to exist before the Sturtian, so the biomarkers hold no specific temporal significance. They do, however, project a diverse community existing during this glaciation associated with a water column stratified with respect to oxygen (which may be due to extensive glaciation resulting in anoxic bottom waters) or oxic waters with a stratified sediment column.

Other studies which interpret an age of Vazante deposition do so in a tectonic framework. All of the rocks within the Brasília Fold Belt (BFB) have been thrust and folded with increasing metamorphic grade to the west, suggesting convergence of the BFB with the São Francisco Craton from that direction (Costa and Angeiras, 1971; Fuck *et al.*, 1994; Dardenne, 2000). In the northern segment, deformation is limited and some depositional contacts remain intact (Dardenne, 2000). Units from the southern segment of the BSB, however, are significantly more deformed into an imbricated series of nappes that have made depositional contacts impossible to decipher (Dardenne, 2000). Since the Vazante Group is within the southern segment, reconstruction of depositional and tectonic environments (which requires interpreting the timing of events) is open to much interpretation and debate.

The two dominant depositional/tectonic models in the literature come from Dardenne (2000) and Pimentel *et al.* (2001). Dardenne (2000) interprets the Vazante sediments to have been deposited in a rapidly subsiding foreland basin similar to the overlying Bambuí Group. In his view, this basin would have formed during development of the initial thrust fronts of the BFB at *ca.* 790 Ma. Carbonates of the Bambuí Group

have been dated at ~740± 20 Ma using Pb-Pb techniques (Babinski and Kaufman, 2003). These particular carbonates exhibit textures that indicate rapid precipitation as sea-floor aragonite fans and are interpreted to be post-glacial cap lithofacies. At the base of the Bambuí Group is a diamictite, which at face value also suggest a possible correlation with the Vazante Group glacial deposits. Our rhenium-osmium dates, however, do not favor this interpretation as the ages are significantly older than the initial thrusting of the BFB and the available radiometric constraints for Bambuí strata.

Based on our ages, the model suggested in Pimentel *et al.* (2001) is preferred (Fig. 22) over that proposed by Dardenne (2000). In their study, Pimentel and others conducted Nd isotopic measurements of detrital grains from different groups within the BFB. From these measurements, the two most likely sources of the sediments of the BFB strata were the São Francisco craton from the east (Nd model ages from ~2.3-1.7 Ga) and the Goiás Magmatic Arc from the west (Nd model ages from ~1.0-1.3 Ga). The Paranoá and Canastra groups are dominated by Paleoproterozoic ages, suggesting deposition there was proximal to the continent and far from the magmatic arc. Detrital grains from the Serra do Garrote and Serra do Poço Verde formations are identical to those of the Paranoá Group (both mostly around 2.03-2.05 Ga) allowing for a similar depositional period and location. The deep water sediments of the Araxá and Ibiá groups have a bimodal distribution suggesting detrital contributions from both the continent and the magmatic arc. The Nd model ages of the Bambuí Group are uniformly spread (i.e., not exhibiting bimodal distribution) throughout the entire range of ~1.9 to 1.3 Ga. This can be explained by mixing of older and younger sources perhaps from a continental arc

due to the thrusting of the BFB to the west (Pimentel *et al.*, 2001), thereby effectively homogenizing the different sources.

The Paranoá Group has been temporally constrained to 1200-900 Ma based on the presence of specific columnar stromatolites (Dardenne *et al.*, 1976), but there are no direct radiometric constraints. The Paranoá Group does, however, sit stratigraphically below the Bamabuí Group in the northern section of the BFB where some depositional contacts are preserved (Dardenne, 2000). Possible associated glacial deposits have also been observed at the base of the Paranoá Group (i.e., the São Miguel paraconglomerate; Dardenne, 2000). Both the Vazante and Paranoá groups have relatively little scatter about 0‰ in $\delta^{13}C_{CARB}$ values, with data ranging from -2.9 to +3.9‰ in the Vazante strata (Azmy *et al.*, 2001) and -3.7 to +2.3‰ in the Paranoá strata (Santos *et al.*, 2000), providing a broad basis for chemostratigraphic equivalence. This is in contrast to carbonates of the Bambuí Group, which exhibits a striking trend in $\delta^{13}C_{CARB}$ values progressing from roughly -5‰ at the base to near +15‰ towards the top of the sequence (Misi *et al*., 2007). These restrictions, along with the Nd isotopic data from Pimentel *et al.* (2001) and the Re-Os ages from this study provide a strong argument that the Vazante Group is correlative with the Paranoá Group and that both groups were deposited on a passive margin >1.0 Ga. Although Rodinia is thought to be a stable supercontinent during this time period, the opening of the Goiás ocean may indicate the break-up of Rodinia was a diachronous process starting as early as 1.0 Ga (Pimentel *et al.*, 2001) with intra-oceanic island arcs developing immediately afterwards (Pimental and Fuck, 1992).

4.2 Implications for "Snowball Earth"

The presence of glendonite and prolific dropstones within the Serra do Poço Verde Formation shales provides robust evidence the sediments were deposited under glacial conditions. Providing the Re-Os age constraints are correct, this would be the only glacial deposit recognized in the Mesoproterozoic Era. Significantly, paleomagnetic data for the Congo-São Francisco craton suggest the conjoined land masses were in tropical latitudes around 1.1 Ga (Fig. 23) as it moved from ~17°N at ~1.2 Ga towards ~40°S at ~1.0 Ga (Tohver *et al.*, 2006). Recent studies provide evidence that there is no single "Sturtian" glacial event, but rather continuous regional glacial events between 750 and 643 Ma (Kendall *et al.*, 2006) or discrete ice ages separated by tens of millions of years (Kaufman *et al.*, 1997). This could indicate the climate during the Neoproterozoic was not cyclical from greenhouse to icehouse with global ice-cover leading to rapid glacial retreat and flooding. Rather, it may have oscillated within each ice age (with each event being similar to the Pleistocene; Leather *et al.*, 2002). The Vazante Group may represent a significantly older series of waxing and waning events akin to what occurred during the Sturtian, and later the Pleistocene. This is consistent with the Vazante stratigraphy seen within the sampled drillcores. Glacially-derived diamictites interbedded with dropstone laden mudstones may indicate pulses of glaciation with the Lapa Formation "cap-carbonate" overlying only the final ice age (Fig. 6).

4.3 Initial $^{187}Os/^{188}Os$ Values

The Re-Os isochrons yield not only the ages of the sample suites, but also initial osmium isotopic compositions. Whereas the osmium is interpreted to be hydrogenous

and has ocean residence times longer than 20,000 years, the initial isotopic composition should reflect that of average seawater osmium. Throughout Earth history, seawater osmium has had $^{187}Os/^{188}Os$ values ranging from chondritic (~0.112) in the Paleoproterozoic (Hannah *et al.*, 2004) to modern values of ~1.06 (Levasseur *et al.*, 1998; Burton *et al.*, 1999; Woodhouse *et al.*, 1999). Although there are large uncertainties, our initial Os isotopic values of 0.12±0.28 for the Serra do Garrote Formation and 0.48±0.15 for the Serra do Poço Verde Formation do fit within expected values for marine osmium. The scatter about the isochrons is most likely attributed to minor variations in the initial osmium composition. Seawater osmium has been documented to track Pleistocene glacial/interglacial cycles (values ranging from 0.94 to 1.06 over 40 ka; Williams and Turekian, 2004) so it can change relatively rapidly. A near chondritic value may indicate a shut-down of continental weathering and the input of radiogenic osmium. This is possible if there were in fact a global glaciation limiting the hydrologic cycle. Low osmium values have also been documented during times of basaltic flood events (Ravizza and Peucker-Ehrenbrink, 2003) when the material being weathered contained a chondritic isotopic composition. Meteorite impacts may also be marked by chondritic excursions in the osmium isotopic record (Ravizza and Peucker-Ehrenbrink, 2003). Introduction of continental material to the oceans via fluvial input would produce a higher (i.e., more radiogenic) signature in the oceans. The large uncertainty of the initial osmium isotopic composition of the Serra do Garrote samples makes it difficult to interpret. The initial osmium isotopic composition of the Serra do Poço Verde samples, however, falls within a range of radiogenic values (0.33 to 0.63). This suggests that continental inputs during the ice age continued, and there would not be a catastrophic shut-down of the hydrologic

cycle during the glaciation. This stands in direct contrast to some hard end-member models of low-latitude glacial events in which global oceans are completely frozen (Hofmann *et al*, 1998b; Hoffman and Schrag, 2002). Other studies have also called for Neoproterozoic regional glaciations on uplifted rift margins during the protracted break-up of Rodinia (Preiss, 2000; Lund *et al.*, 2003; Eyles and Januszczak, 2004), as opposed to global ice cover.

4.4 Significance of Model Ages

Since the rhenium and osmium measured in the samples are hydrogenous, the model ages simply provide support for closed system behavior. Total analytical duplicates do not perfectly repeat themselves. This may be the result of either open system behavior skewing the values, or powder heterogeneities within a closed system. For example, sample 825.86Cr was analyzed six times (Table 5). Although $^{187}Re/^{188}Os$ values range from ~180 to ~200, the model ages range only from 1.30 to 1.35 Ga. This reproducibility of model ages suggests the observed variance is isochronous. If an isochronous relationship is preserved it is unlikely the samples have experienced any open system conditions. On the other hand, sample 803.89 was analyzed two times with model ages of 1.28 and 1.55 Ga, despite reproducing $^{187}Os/^{188}Os$ values of 1.86 and 1.88 (Table 7). It is likely, therefore, that this bulk powder has experienced some open system behavior. Due to the generally good reproducibility of model ages within duplicates (particularly within samples from the Serra do Poço Verde Fm.), scatter about the isochrons are attributed to minor variations in the initial $^{187}Os/^{188}Os$ values between samples.

The errorchrons produced from samples of the Lapa Fm. (Table 8) and samples M1Cr-M5Cr (Table 6) are likely a product of open system behavior within the samples. Both of these sample sets exhibit poor reproducibility of model ages within duplicates and between samples.

4.5 Stable Isotopes and Elemental Abundances

All three drillcores exhibit remarkable preservation of organic matter in discrete horizons. Insofar that organic carbon preservation is likely to be associated with reducing conditions, higher TOC abundance samples have a higher likelihood of being able to sequester rhenium and osmium from seawater. Hayes *et al.* (1983) notes that a negative trend in TOC abundance vs. isotopic composition could be explained by thermally maturing the shales during diagenesis. If all samples have the same initial organic carbon isotopic compsition and abundance, then burning off carbon would preferentially remove the lighter isotope, causing organic-lean material to be isotopically heavier. This trend is not recognized in these samples (Fig. 24).

It is difficult to interpret the isotopic data of reduced components (i.e., organic carbon and residual sulfide) fully as we do not have information on the isotopic composition of the oxidized counterparts (i.e. inorganic carbon and the initial sulfate pool). Partly, this is because there is negligible amount of carbonate in the studied shale intervals where such information could be procured. Assuming carbonate carbon has a $\delta^{13}C$ value around 0‰ (true values may range from +4 to -4‰, as seen in Azmy *et al.*, 2001), the $\delta^{13}C$ values of the organic matter also fall within expected values of Proterozoic organic matter in all three drillcores (similar values to Azmy *et al.*, 2006).

We do, however, see opposing trends between the carbon and sulfur isotopes within the Serra do Poço Verde Formation in drillcore 134-86 (Fig. 25). This is the thickest section we have within this well analyzed drillcore (~100 meters, versus ~30 meters of the Serra do Garrote Formation and ~50 meters of the Lapa Formation). One possible interpretation of these opposing trends is the redox sensitivity of the bacteria driving the fractionation. Heavier carbon isotopes (a shift towards the right) may suggest that prolific carbon fixation was occurring. Since oxygen is a product of photosynthetic carbon fixation, the water column may have been oxidizing. Sulfate-reducing bacteria, however, thrive in reducing environments (Fenchel *et al.*, 1998). Therefore they would be unable to occupy the water column, and be driven into the sediment column. With their capacity to reduce sulfate diminished, more fractionation (i.e., lighter residual sulfide sulfur) would be expected. Alternatively, rapid carbon fixation, and subsequent oxygen production, would increase the proportion of sulfur existing as sulfate. High sulfate concentrations would allow sulfate-reducing bacteria to be more selective and increase kinetic isotope effects, thus producing lighter residual sulfide. Regardless of which environmental scenario is correct, either would produce the relationship we see within the Serra do Poço Verde Formation.

There is robust evidence that life was not catastrophically affected as some models of Proterozoic glaciations predict (Hoffman *et al*, 1998). Interactions between different metabolic processes in the isotope record, abundant preservation of organic matter, expected isotopic compositions of bacterially-driven fractionation, and the presence of photosynthetic bacteria (Olcott *et al.*, 2005) indicates an active photic zone calling for little to no ice cover in the basin.

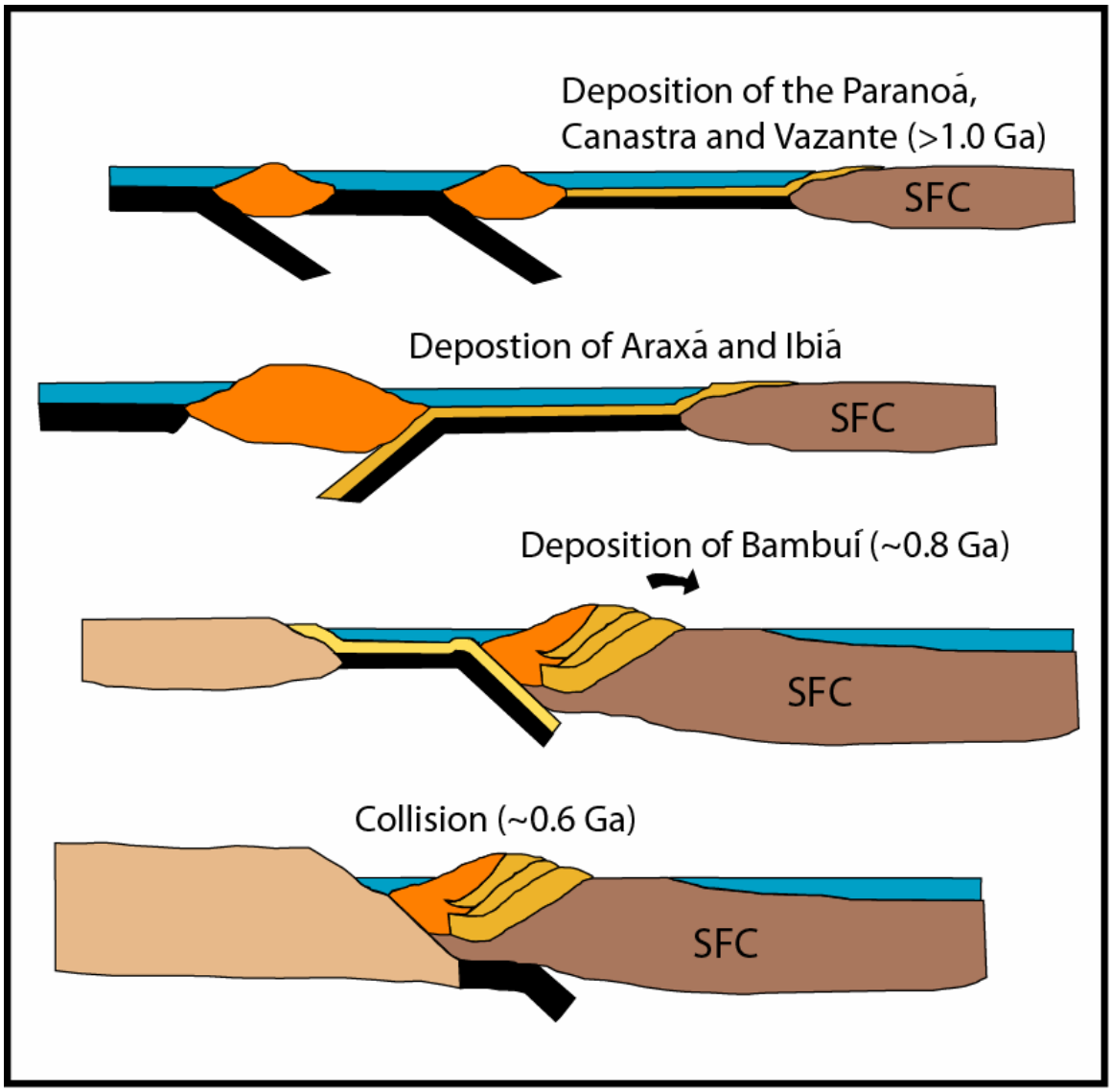

Figure 22. Depositional and tectonic model for the Vazante Group with respect to the events of the Brasiliá Fold Belt (modified from Pimentel et al., 2001). SFC is São Francisco Craton.

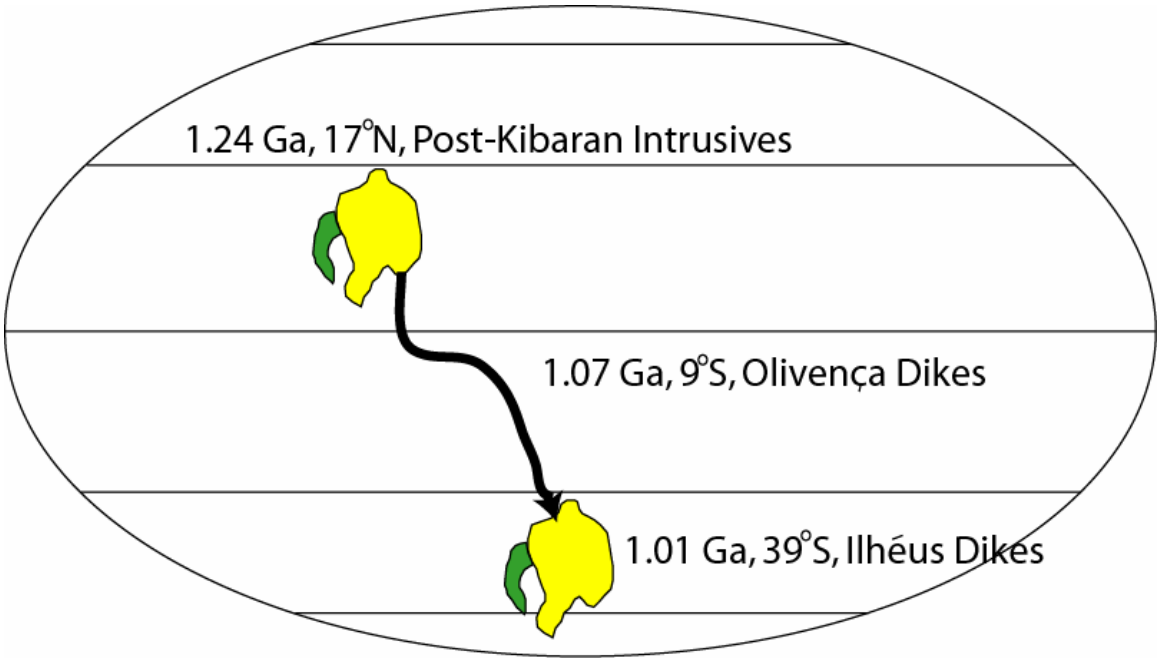

Figure 23. Paleolatitude movement of the São Francisco-Congo Craton during the Mesoproterozoic. The rotational axis of the landmass is not accounted for. The Congo is in yellow while the São Francisco is in green. Modified from Tohver *et al*., 2006.

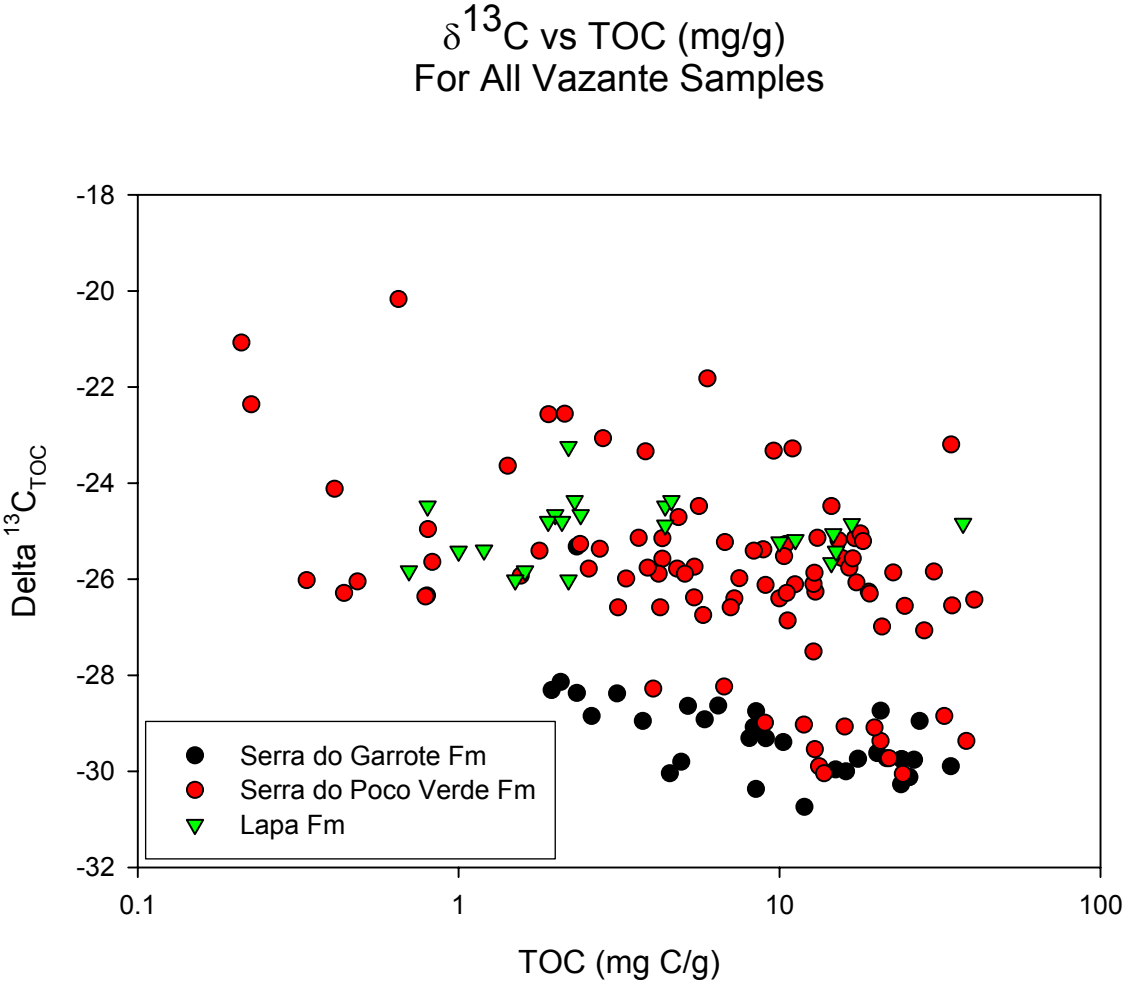

Figure 24. Total organic carbon abundance vs. isotopic composition of the organic carbon for shale samples from drillcore 134-86. The lack of a pronounced negative trend suggests the spread in values is not due to thermal maturation.

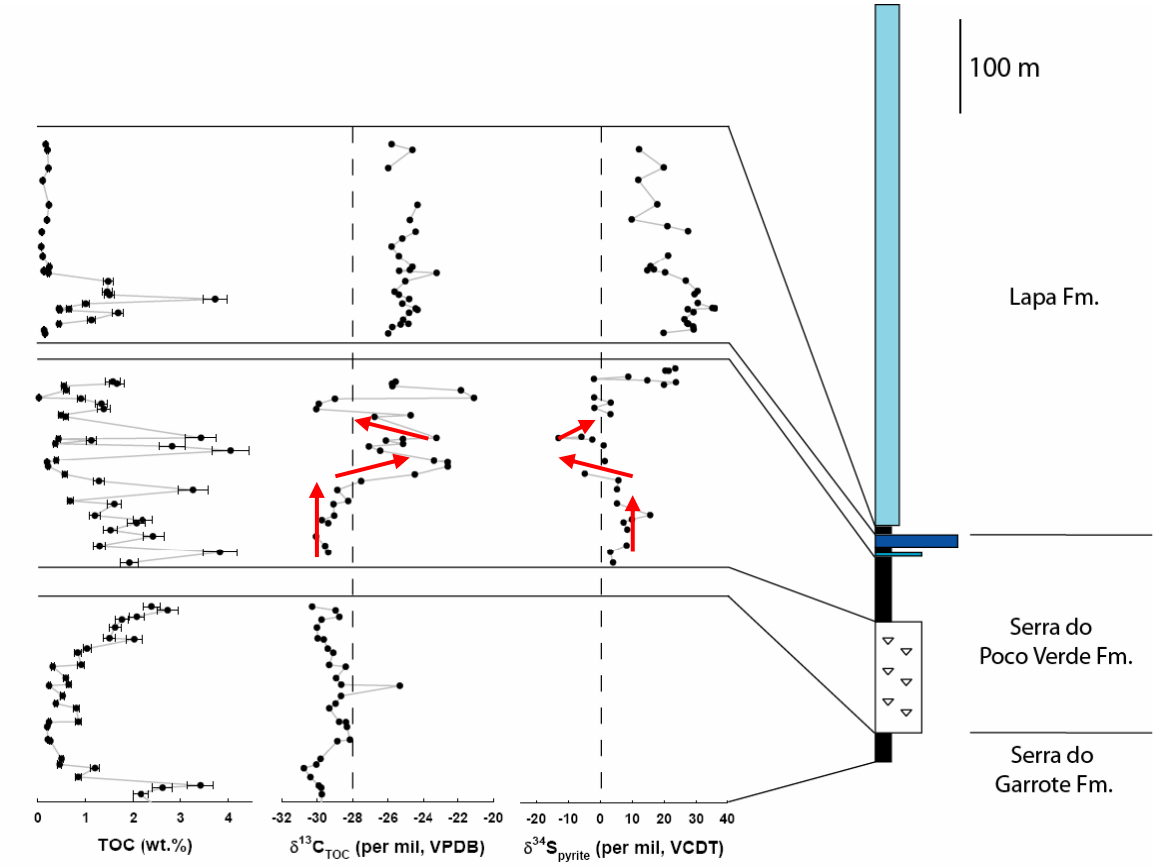

Figure 25. Isotopic and elemental abundance data for shale horizons within the Vazante Group in drillcore 134-86. Note the generally opposing trends of organic carbon and sulfide sulfur interpreted to reflect activity of obligate metabolisms active during the glacial event.

Chapter 5: Conclusions

The Re-Os age constraints from this study indicate that the Vazante Formation was not deposited during Neoproterozoic glaciation (*cf.* Azmy *et al*., 2001; Olcott *et al.*, 2005; Azmy *et al.*, 2006). Rather, they place the Vazante Group sediments in the latest Mesoproterozoic Era between *ca.* 1300 and 1100 Ma. Nontheless, the presence of glendonite and dropstones within the Serra do Poço Verde shales do provide evidence that parts of the Vazante strata were deposited during an ice age. Thus far, no other glacial deposit has been recognized during this time period. However, recent studies have suggested that there is no single "Sturtian" glacial event, but rather several local events, representing ice sheets forming on uplifted rift margins during the protracted break-up of Rodinia (Kendall *et al.*, 2006). The Vazante diamictites may similarly represent an ice sheet formed during a much earlier (late Mesoproterozoic) rifting event off the western edge of the São Francisco craton, with the glaciers advancing to the sea.

With these new age constraints, the Vazante Group is correlative with the Paranoá Group within the Brasiliá Fold Belt. The presence of columnar stromatolites that restrict the age from 1350-950 Ma (Cloud and Dardenne, 1973) within both the Vazante and Paranoá groups, as well as carbon isotopic comparisons, further corroborate this correlation. The preferred depositional and tectonic setting for the Vazante Group is that from Pimentel and others (2001) in which the Vazante, Paranoá and Canastra groups were deposited on a passive margin following a partial early break-up of Rodinia before 1.0 Ga.

Stable isotopic and organic carbon abundances within Vazante shales suggest bacterial communities were active during the glaciation. This stands in stark contrast to some hard-end models that call for a complete shutdown of primary productivity during Proterozoic glacial events (as in Hoffman *et al*., 1998). Therefore, it appears that during the Mesoproterozoic Vazante ice age sea-ice was not extensive enough to have eliminated the photic zone within the shallow ocean basin.

The Proterozoic "climate paradox" remains unresolved. It is difficult to say what circumstances must be in balance to have the conditions needed for glaciation at equatorial latitudes. Does the Vazante Group represent a tectonically driven local glacial event, or is it the only window into a possible biologically driven global glacial event? Kah and others (1999) show moderate swings (relative to those in the Neoproterozoic) in the carbon isotopic composition of carbonates (~7‰) during the late Mesoproterozoic Era (Fig. 26). If the negative $\delta^{13}C$ excursions of that era are also related to glaciation, it could indicate that biology progressively drove the Earth into a state primed for glaciation, and perhaps regional tectonics pushed various regions past the tipping point. The presence of glendonite would require glaciers not only above the snow line, but frigid shelf-waters as well. The lithologic oscillation from diamictite to shale/carbonate suggests the ice-sheets waxed and waned, perhaps similarly to Pleistocene events. While this study does not resolve a mechanism for glaciation, it does provide for the strong possibility that the environmental conditions present during the Neoproterozoic extend further back in Earth history than previously thought.

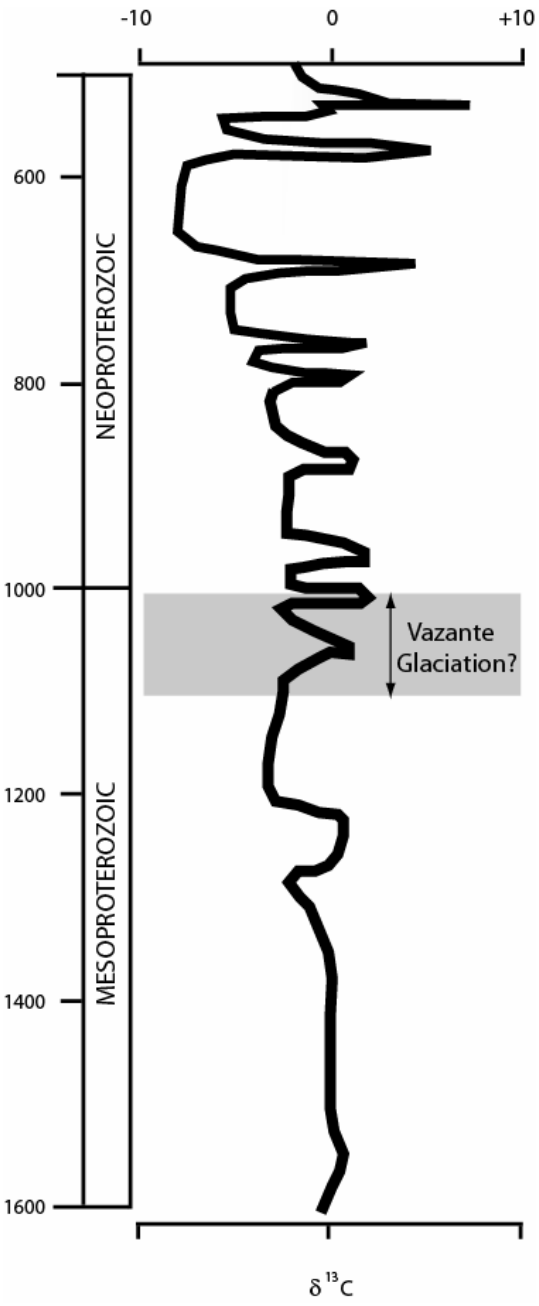

Figure 26. Carbonate carbon isotopic composition during the Meso- and Neoproterozoic. The large swings in the Neoproterozoic are associated with low-latitude glaciation. Relatively muted swings in $\delta^{13}C$ are also seen in the Mesoproterozoic, perhaps due to smaller, but similar, events. Modified from Kah *et al*, 1999.

Appendix A

A-1: Digestion

1. Approximately 50mg of powdered whole rock is accurately weighed and transferred into a pyrex carius tube, along with a known amount of ^{190}Os and ^{185}Re spikes and the tubes are placed into an ice bath. The mass of the spike is determined by attempting to double the natural ratio of $^{190}Os/^{192}Os$ and $^{185}Re/^{187}Re$.
2. Approximately 6g of inverse aqua regia **OR** 4mL of chromic-oxide dissolved in sulfuric acid (0.2g/mL 12N acid) is added into the carius tube and the tube is sealed with an oxygen-fed torch.
3. The carius tubes are placed in metal jackets and placed in a 240°C oven for 48 hours.

A-2: Osmium Separation and Purification

1. When cool, the tubes are chilled in liquid nitrogen and opened. The contents are added to 50mL centrifuge tubes along with 3mL of carbon tetrachloride. Shake the contents for 60 seconds, then centrifuge.
2. Pipette out the denser carbon tetrachloride and add to a 15mL Teflon beaker along with 4mL of concentrated hydrobromic acid.
3. Repeat steps 1 and 2. Save centrifuge tube contents of remaining inverse aqua regia or chromic oxide/sulfuric acid.

4. Seal Teflon beaker that contains HBr and carbon tetrachloride and place on ~80°C hot plate overnight.
5. When cool, transfer denser carbon tetrachloride from bottom of Teflon beaker to appropriate waste container. Dry remaining HBr under heat lamp until only a small drop remains (~40μL).
6. Transfer the drop of HBr to the inside of a cap of a 5mL conical Teflon vial and dry completely.
7. Place a 15μL drop of concentrated HBr into the bottom of a 5mL conical Teflon vial so the surface tension holds it in place. Add ~30μL of dichromate over the dried HBr on the cap and invert the bottom section over the top and screw on.
8. Wrap the vial in aluminum foil so that only the conical bottom (physically on top) with the drop of HBr remains uncovered. Place on ~100°C hot plate and distill for 2-3 hours.
9. Remove rinse off dichromate. Recap and let sit 1 hour to ensure all Os is reduced. Dry down completely. Add ~1.0μL of concentrated HBr. Ready to analyze.

A-3: Rhenium Separation

1. Following Os separation, inverse aqua regia is transferred to a clean 15mL Teflon vial and dried down completely under a heat lamp. If using chromic-oxide/sulfuric acid, the solution must first be reduced. Approximately 2mL of sulfurous acid is added for every 1mL solution. Dry down and repeat.
2. The dry reagent is then taken up in 10mL of 0.8N nitric acid and left on a ~80°C hot plate for several hours (or overnight).
3. Once cool, the following scheme is used in a 2mL Biorad column filled with 1.7mL of AG1x8 resin:

   Elute 10mL of Milli-Q
   Elute 2.5mL of 0.8N Nitric Acid
   Elute 2x 10mL 6N Nitric Acid (first time quartz distilled, second time Teflon distilled)
   Elute 3mL 0.8N Nitric Acid
   Load and elute sample (in 10mL 0.8 Nitric Acid)
   Elute 2.5mL 1N Hydrochloric Acid
   Elute 7.5mL 1N Hydrochloric Acid
   Elute 2.5mL 0.8N Nitric Acid
   Elute 2.0mL 6N Nitric Acid
   Collect in 10mL 6N Nitric Acid in 15mL Teflon vial. Dry down completely.

4. Take-up in 1mL 0.8N Nitric Acid and place on ~100°C hot plate for 1-2 hours.
5. Pass through 0.25mL polyethylene columns filled with AG1x8 anion resin with the following scheme:

Elute 5mL Milli-Q

Elute 2mL 0.8N Nitric Acid

Elute 3x 3mL 6N Nitric Acid

Equilibrate with 2mL 0.8N Nitric Acid

Load and elute sample (in 1mL 0.8N Nitric Acid)

Elute 2x 1mL 0.8N Nitric Acid

Collect Re in 4mL 6N Nitric Acid in rinsed 15mL Teflon vials. Dry down.

Add 2-3 drops both concentrated Nitric and Hydrochloric Acids. Dry down.

6. Take up in 0.5mL 2% Nitric Acid. Ready to analyze on ICP-MS.

Appendix B

Running conditions for elemental analyzer-gas chromatograph-mass spectrometer:

	Carbon Isotopes	Sulfur Isotopes
Carrier (kPa)	65	85
Purge (mL/min)	80	60
Oxygen Volume (mL)	10	15
Oxygen Δpressure	30	25
Time (sec)	5	9.3
SMP (sec)	50	12
Run (sec)	320	93
Front Oven (°C)	1020-1040	1030
Rear Oven (°C)	650	OFF
GC Column (°C)	115	100

Bibliography

Amaral, G., and Kawashita, K., 1967, Determinação da idade do Grupo Bambuí pelo métado Rb/Sr in Congresso Brasileiro Geologia 21, Anais, SBG, pp. 214-217.

Azmy, K., Kaufman, A.J., Misi, A., and de Oliveira, T.F., 2006, Isotope stratigraphy of the Lapa Formation, Sao Francisco Basin, Brazil: Implications for Late Neoproterozoic glacial events in South America: Precambrian Research, v. 149, p. 231-248.

Azmy, K., Veizer, J., Misi, A., de Oliveira, T.F., Sanches, A.L., and Dardenne, M.A., 2001, Dolomitization and isotope stratigraphy of the Vazante Formation, Sao Francisco Basin, Brazil: Precambrian Research, v. 112, p. 303-329.

Babinski, M., and Kaufman, A.J., 2003, First direct dating of a Neoproterozoic post-glacial cap carbonate, South American Symposium on Isotope Geology 4, Short Papers 1, pp. 321-23.

Babinski, M., Monteiro, L.S., Fetter, A.H., Bettencourt, J.S., and Oliveira, T.F., 2005, Isotope geochemistry of the mafic dikes from the Vazante nonsulfide zinc deposit, Brazil: Journal of South American Earth Sciences, v. 18, p. 293-304.

Bekker, A., Kaufman, A.J., Karhu, J.A., and Eriksson, K.A., 2005, Evidence for Paleoproterozoic cap carbonates in North America: Precambrian Research, v. 137, p. 167-206.

Bodiselitsch, B., Koeberl, C., Master, S., and Reimold, W.U., 2005, Estimating duration and intensity of Neoproterozoic snowball glaciations from Ir anomalies: Science, v. 308, p. 239-242.

Bowring, S.A., Grotzinger, J.P., Isachsen, C.E., Knoll, A.H., Pelechaty, S.M. and Kolosov, P., 1993, Calibrating rates of early Cambrian evolution: Science, v. 261, n. 5126, pp. 1293-1298.

Bowring, S.A., and Schmitz, M.D., 2003, High-precision U-Pb zircon geochronology and the stratigraphic record, Zircon, Volume 53: Reviews in Mineralogy & Geochemistry, p. 305-326.

Brody, K.B., et al., 2004, Biomarker geochemistry of a post-glacial Neoproterozoic succession in Brazil, Geological Society of America Abstracts with Programs, Vol. 36, No. 5, p. 477.

Burton, K.W., Bourdon, B., Birck, J.L., Allegre, C.J., and Hein, J.R., 1999, Osmium isotope variations in the oceans recorded by Fe-Mn crusts: Earth and Planetary Science Letters, v. 171, p. 185-197.

Caldeira, K., and Kasting, J.F., 1992, Susceptibility of the Early Earth to Irreversible Glaciation Caused by Carbon-Dioxide Clouds: Nature, v. 359, p. 226-228.

Canfield, D.E., Raiswell, R., Westrich, J.T., Reaves, C.M., and Berner, R.A., 1986, The Use of Chromium Reduction in the Analysis of Reduced Inorganic Sulfur in Sediments and Shales: Chemical Geology, v. 54, p. 149-155.

Cloud, P., and Dardenne, M., 1973, Proterozoic Age of Bambui Group in Brazil: Geological Society of America Bulletin, v. 84, p. 1673-1676.

Cohen, A.S., 2004, The rhenium-osmium isotope system: applications to geochronological and palaeoenvironmental problems: Journal of the Geological Society, v. 161, p. 729-734.

Cohen, A.S., Coe, A.L., Bartlett, J.M., and Hawkesworth, C.J., 1999, Precise Re-Os ages of organic-rich mudrocks and the Os isotope composition of Jurassic seawater: Earth and Planetary Science Letters, v. 167, p. 159-173.

Costa, L.A.M. and Angeiras, A.G>, 1971, Geosynclinal evolution in the epi-Baikalian platform of Central Brazil, Geologische Rundshau, v. 60, n. 2, pp. 1024-1050.

Creaser, R.A., Sannigrahi, P., Chacko, T., and Selby, D., 2002, Further evaluation of the Re-Os geochronometer in organic-rich sedimentary rocks: A test of hydrocarbon maturation effects in the Exshaw Formation, Western Canada Sedimentary Basin: Geochimica Et Cosmochimica Acta, v. 66, p. 3441-3452.

Dardenne, M.A., 2000, The Brasília Fold Belt in Tectonic Evolution of South America, edited by Cordani, U.G., Milani, E.J., Filho, A.T., and Campos, D.A., pp. 231-263, 31st International Geological Congress, Rio de Janeiro.

Dardenne, M.A., Faria, A., and Andrade, G.F., 1976, Occurence de stromatolithes collumnaires dans le Groupe Bambuí (Goiás, Brésil), Anais da Academia Brasileira de Ciências, v. 48, n. 3, pp. 555-566.

Dickin, A.P., 1995, Radiogenic Isotope Geology, Cambridge University Press, Cambridge, 490p.

Evans, D.A.D., 2000, Stratigraphic, geochronological, and paleomagnetic constraints upon the neoproterozoic climatic paradox: American Journal of Science, v. 300, p. 347-433.

Eyles, N., and Januszczak, N., 2004, 'Zipper-rift': a tectonic model for Neoproterozoic glaciations during the breakup of Rodinia after 750 Ma: Earth-Science Reviews, v. 65, p. 1-73.

Faure, G., 1991, Principles and Applications of Geochemistry (2nd Ed.), Prentice Hall, Upper Saddle River, New Jersey, 600p.

Fuck, R.A., Pimentel, M.M., and Silva, J.H.D, 1994, Compartmentação tectônica na porção oriental da Provía Tocantins in Congresso Brasileiro Geologia 38, Anais, SBG, pp. 215-216.

Fenchel, T., King, G.M., and Blackburn, T.H., 1998, Bacterial Biogeochemisty: The Ecophysiology of Mineral Cycling (2nd Ed.), Elsevier Academic Press, San Diego, California, 307p.

Habicht, K.S., and Canfield, D.E., 2001, Isotope fractionation by sulfate-reducing natural populations and the isotopic composition of sulfide in marine sediments: Geology, v. 29, p. 555-558.

Hannah, J.L., Bekker, A., Stein, H.J., Markey, R.J., and Holland, H.D., 2004, Primitive Os and 2316 Ma age for marine shale: implications for Paleoproterozoic glacial events and the rise of atmospheric oxygen: Earth and Planetary Science Letters, v. 225, p. 43-52.

Harland, W.B., and Bidgood, D.E.T., 1959, Palaeomagnetism in Some Norwegian Sparagmites and the Late Pre-Cambrian Ice Age: Nature, v. 184, p. 1860-1862.

Hayes, J.M., Kaplan, I.R., Wedeking, K.W., 1983, Precambrian organic geochemistry preservation of the record in Earth's Earliest Biosphere: Its Origin and Evolution, edited by Schopf, J.W., Princeton University Press, Princeton, NJ, 543p.

Hoffman, P.F., 1999, The break-up of Rodinia, birth of Gondwana, true polar wander and the snowball Earth: Journal of African Earth Sciences, v. 28, p. 17-33.

Hoffman, P.F., Kaufman, A.J., Halverson, G.P., and Schrag, D.P., 1998a, A Neoproterozoic snowball earth: Science, v. 281, p. 1342-1346.

Hoffman, P.F., Kaufman, A.J., Halverson, G.P., and Schrag, D.P., 1998b, Comings and Goings of Global Glaciations on a Neoproterozoic Tropical Platform in Namibia: GSA Today, v. 8, n. 5, p. 1-9.

Hoffman, P.F., and Schrag, D.P., 2002, The snowball Earth hypothesis: testing the limits of global change: Terra Nova, v. 14, p. 129-155.

Hsieh, Y.P., and Sheih, Y.N., 1997, Analysis of reduced inorganic sulfur by diffusion methods: improved apparatus and evaluation for sulfur isotopic studies: Chemical Geology, v. 137, pp. 255-261.

Hsieh, Y.P. and Yang, C.H., 1989, Diffusion methods for the determination of reduced inorganic sulfur species in sediments: Limnology and Oceanography, v. 34, pp. 1126-1130.

Hurtgen, M.T., Arthur, M.A., and Halverson, G.P., 2005, Neoproterozoic sulfur isotopes, the evolution of microbial sulfur species, and the burial efficiency of sulfide as sedimentary pyrite: Geology, v. 33, p. 41-44.

Jaffe, L.A., Peucker-Ehrenbrink, B., and Petsch, S.T., 2002, Mobility of rhenium, platinum group elements and organic carbon during black shale weathering: Earth and Planetary Science Letters, v. 198, p. 339-353.

James, N.P., Narbonne, G.M., Dalrymple, R.W., and Kyser, T.K., 2005, Glendonites in neoproterozoic low-latitude, interglacial, sedimentary rocks, northwest Canada: Insights into the Cryogenian ocean and Precambrian cold-water carbonates: Geology, v. 33, p. 9-12.

Kah, L.C., Sherman, A.G., Narbonne, G.M., Knoll, A.H., and Kaufman, A.J., 1999, $\delta^{13}C$ stratigraphy of the Proterozoic Bylot supergroup, Baffin Island, Canada: implications for regional lithostratiraphic correlations: Canadian Journal of Earth Science, v. 36, pp. 313-332.

Kaufman, A.J., Hayes, J.M., Knoll, A.H., and Germs, G.J.B., 1991, Isotopic compositions of carbonates and organic-carbon from upper Proterozoic successions in Namibia-Stratigraphic variation and the effects of diagenesis and metamorphism: Precambrian Research, v. 49, n. 3-4, pp. 301-327.

Kaufman, A.J., and Knoll, A.H., 1995, Neoproterozoic Variations in the C-Isotopic Composition of Seawater - Stratigraphic and Biogeochemical Implications: Precambrian Research, v. 73, p. 27-49.

Kaufman, A.J., Knoll, A.H., and Awramik, S.M., 1992, Biostratigraphic and Chemostratigraphic Correlation of Neoproterozoic Sedimentary Successions - Upper Tindir Group, Northwestern Canada, as a Test Case: Geology, v. 20, p. 181-185.

Kaufman, A.J., Knoll, A.H., and Narbonne, G.M., 1997, Isotopes, ice ages, and terminal Proterozoic earth history: Proceedings of the National Academy of Sciences of the United States of America, v. 94, p. 6600-6605.

Kendall, B., Creaser, R.A., and Selby, D., 2006, Re-Os geochronology of postglacial black shales in Australia: Constraints on the timing of "Sturtian" glaciation: Geology, v. 34, p. 729-732.

Kendall, B.S., Creaser, R.A., Ross, G.M., and Selby, D., 2004, Constraints on the timing of Marinoan "Snowball Earth" glaciation by Re-187-Os-187 dating of a Neoproterozoic, post-glacial black shale in Western Canada: Earth and Planetary Science Letters, v. 222, p. 729-740.

Kennedy, M.J., 1996, Stratigraphy, sedimentology, and isotopic geochemistry of Australian Neoproterozoic postglacial cap dolostones: Deglaciation, delta C-13 excursions, and carbonate precipitation: Journal of Sedimentary Research, v. 66, p. 1050-1064.

Kennedy, M.J., Christie-Blick, N., and Sohl, L.E., 2001, Are Proterozoic cap carbonates and isotopic excursions a record of gas hydrate destabilization following Earth's coldest intervals?: Geology, v. 29, p. 443-446.

Kennedy, M.J., Runnegar, B., Prave, A.R., Hoffmann, K.H., and Arthur, M.A., 1998, Two or four Neoproterozoic glaciations?: Geology, v. 26, p. 1059-1063.

Kirschvink, J.W., 1992, Late Proterozoic low-latitude global glaciations: the Snowball Earth, in The Proterozoic Biosphere, edited by J.W. Schopf and C. Klein, pp. 51-52, Cambridge University Press, Cambridge.

Knoll, A.H., Hayes, J.M., Kaufman, A.J., Swett, K., and Lambert, I.B., 1986, Secular Variation in Carbon Isotope Ratios from Upper Proterozoic Successions of Svalbard and East Greenland: Nature, v. 321, p. 832-838.

Kroner, A., and Cordani, U., 2003, African, southern Indian and South American cratons were not part of the Rodinia supercontinent: evidence from field relationships and geochronology: Tectonophysics, v. 375, p. 325-352.

Leather, J., Allen, P.A., Brasier, M.D., and Cozzi, A., 2002, Neoproterozoic snowball earth under scrutiny: Evidence from the Fiq glaciation of Oman: Geology, v. 30, p. 891-894.

Levasseur, S., Birck, J.L., and Allegre, C.J., 1998, Direct measurement of femtomoles of osmium and the Os-187/Os-186 ratio in seawater: Science, v. 282, p. 272-274.

Lund, K., Aleinikoff, J.N., Evans, K.V., and Fanning, C.M., 2003, SHRIMP U-Pb geochronology of neoproterozoic Windermere Supergroup, central Idaho: Implications for rifting of western Laurentia and synchroneity of Sturtian glacial deposits: Geological Society of America Bulletin, v. 115, p. 349-372.

Misi, A., Kaufman, A.J., Veizer, J., Powis, K., Azmy, K., Boggiana, P.C., Gaucher, C., Teixeira, J.B.G., Sanches, A.L., and Iyer, S.S.S., 2007, Chemostratigraphic correlation of Neoproterozoic successions in South America: Chemical Geology, doi: 10.1016/j.chemgeo.2006.06.019.

Olcott, A.N., Sessions, A.L., Corsetti, F.A., Kaufman, A.J., and de Oliviera, T.F., 2005, Biomarker evidence for photosynthesis during Neoproterozoic glaciation: Science, v. 310, p. 471-474.

Oxburgh, R., 2001, Residence time of osmium in the oceans: Geochemistry Geophysics Geosystems, 2.

Peucker-Ehrenbrink, B., and Ravizza, G., 2000, The marine osmium isotope record: Terra Nova, v. 12, p. 205-219.

Peuckerehrenbrink, B., Ravizza, G., and Hofmann, A.W., 1995, The Marine Os-187/Os-186 Record of the Past 80-Million Years: Earth and Planetary Science Letters, v. 130, p. 155-167.

Pimentel, M.M., Dardenne, M.A., Fuck, R.A., Viana, M.G., Junges, S.L., Fischel, D.P., Seer, H.J., and Dantas, E.L., 2001, Nd isotopes and the provenance of detrital sediments of the Neoproterozoic Brasilia Belt, central Brazil: Journal of South American Earth Sciences, v. 14, p. 571-585.

Pimentel, M.M., and Fuck, R.A., 1992, Neoproterozoic Crustal Accretion in Central Brazil: Geology, v. 20, p. 375-379.

Plumb, K.A., 1991, New Precambrian Time Scale: Episodes, v. 14, p. 139-140.

Preiss, W.V., 2000, The Adelaide Geosyncline of South Australia and its significance in Neoproterozoic continental reconstruction: Precambrian Research, v. 100, p. 21-63.

Ravizza, G., and Esser, B.K., 1993, A Possible Link between the Seawater Osmium Isotope Record and Weathering of Ancient Sedimentary Organic-Matter: Chemical Geology, v. 107, n. 3-4, pp. 255-258.

Ravizza, G., and Peucker-Ehrenbrink, B., 2003, Chemostratigraphic evidence of Deccan volcanism from the marine osmium isotope record: Science, v. 302, p. 1392-1395.

Ravizza, G., and Turekian, K.K., 1989, Application of the Re-187-Os-187 System to Black Shale Geochronometry: Geochimica Et Cosmochimica Acta, v. 53, p. 3257-3262.

Santos, R.V., de Alvarenga, C.J.S., Dardenne, M.A., Sial, A.N., and Ferreira, V.P., 2000, Carbon and oxygen isotope profiles across Meso-Neoproterozoic limestones from central Brazil: Bambuí and Paranoá groups: Precambrian Research, v. 104, pp. 107-122.

Schaefer, B.F., and Burgess, J.M., 2003, Re-Os isotoic age constraints on deposition in the Neoproterozoic Amadeus Basin: implications for the 'Snowball Earth': Journal of the Geological Society, v. 160, p. 825-828.

Schrag, D.P., Berner, R.A., Hoffman, P.F., and Halverson, G.P., 2002, On the initiation of a snowball Earth: Geochemistry Geophysics Geosystems, v. 3.

Selby, D., and Creaser, R.A., 2003, Re-Os geochronology of organic rich sediments: an evaluation of organic matter analysis methods: Chemical Geology, v. 200, p. 225-240.

Selby, D., and Creaser, R.A., 2005, Direct radiometric dating of hydrocarbon deposits using rhenium-osmium isotopes: Science, v. 308, p. 1293-1295.

Shirey, S.B., and Walker, R.J., 1995, Carius Tube Digestion for Low-Blank Rhenium-Osmium Analysis: Analytical Chemistry, v. 67, p. 2136-2141.

Shirey, S.B., and Walker, R.J., 1998, The Re-Os isotope system in cosmochemistry and high-temperature geochemistry: Annual Review of Earth and Planetary Sciences, v. 26, p. 423-500.

Tohver, E., D'Agrella, M.S., and Trindade, R.I.F., 2006, Paleomagnetic record of Africa and South America for the 1200-500 Ma interval, and evaluation of Rodinia and Gondwana assemblies: Precambrian Research, v. 147, p. 193-222.

Walker, R.J., 1988, Low-Blank Chemical-Separation of Rhenium and Osmium from Gram Quantities of Silicate Rock for Measurement by Resonance Ionization Mass-Spectrometry: Analytical Chemistry, v. 60, p. 1231-1234.

Walter, M.R., Veevers, J.J., Calver, C.R., Gorjan, P., and Hill, A.C., 2000, Dating the 840-544 Ma Neoproterozoic interval by isotopes of strontium, carbon, and sulfur in seawater, and some interpretative models: Precambrian Research, v. 100, p. 371-433.

Williams, G.A., and Turekian, K.K., 2004, The glacial-interglacial variation of seawater osmium isotopes as recorded in Santa Barbara Basin: Earth and Planetary Science Letters, v. 228, p. 379-389.

Woodhouse, O.B., Ravizza, G., Kenison-Falkner, K., Statham, P.J., and Peucker-Ehrenbrink, B., 1999, Osmium in seawater: vertical profiles of concentration and isotopic composition in the eastern Pacific Ocean: Earth and Planetary Science Letters, v. 173, p. 223-233.